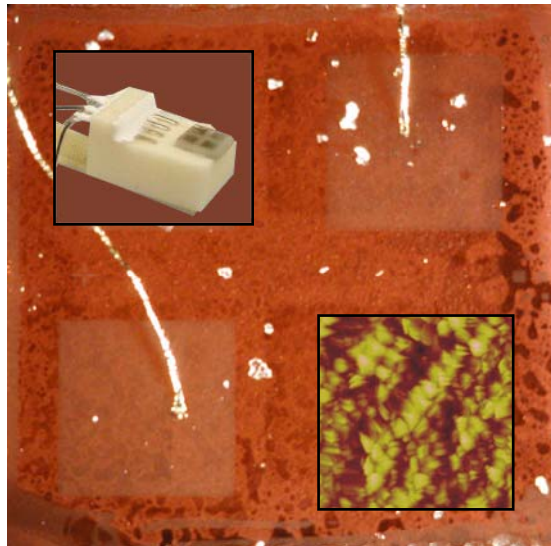




**University of Twente**  
*The Netherlands*

# **Ionic Conductivity in Yttria-Stabilized Zirconia Thin Films grown by Pulsed Laser Deposition**



Jetske Karina Stortelder  
Master of Science Thesis  
Faculty of Science and Technology  
Inorganic Materials Science  
Mesa+ Institute for Nanotechnology  
Enschede, August 2005



# **Ionic Conductivity in Yttria-Stabilized Zirconia Thin Films grown by Pulsed Laser Deposition**

**Master of Science Thesis by  
Jetske Karina Stortelder  
Enschede, August 26<sup>th</sup> 2005**

Graduation Committee

Prof. Dr. Ing. D.H.A. Blank

Dr. Ing. A.J.H.M. Rijnders

Ir. F. Vroegindeweyj

Dr. H.J.M. Bouwmeester

Dr. B.J. Ravoo

Dr. Ir. B. Timmer (Texas Instruments)



## Summary

In this report the ionic conductivity of yttria-stabilized zirconia (YSZ) is researched. YSZ transports oxygen through its lattice and can, for example, be used for the detection of oxygen and, indirectly, for harmful  $\text{NO}_x$  gasses that contribute to environmental problems.

The objective of this research was to determine the influence of the crystal structure on the ionic conductivity of YSZ thin films produced by pulsed laser deposition. The materials used for the electrodes and wiring of the samples, the measurement set-up and the sample configuration played an important role in obtaining successful impedance measurements in temperatures up to  $900^\circ\text{C}$ . Part of this research was therefore contributed to finding the optimal conditions for ionic conductivity measurements on YSZ thin films.

Four electrode materials were chosen and tested, knowing  $\text{SrRuO}_3$ , Pt, Au and Pt-paste, but only  $\text{SrRuO}_3$  and Pt were useful until  $700^\circ\text{C}$ . After that temperature the films started to segregate, which reduced the electrode contact area and increased the resistance. So none of the electrode materials was suitable to measure up to  $900^\circ\text{C}$  in an oxygen environment. However, the results obtained from low temperature measurements can be extrapolated to higher temperatures to get an indication of the values at high temperatures. For the wiring gold was used.

YSZ thin films were deposited on  $\text{SrTiO}_3$  as well as on  $\text{NdGaO}_3$ , resulting in different crystallinities. On  $\text{NdGaO}_3$ , the YSZ was deposited epitaxial in the  $[001]$  directions and on the  $\text{SrTiO}_3$  in the  $[011]$  and  $[001]$  directions. The activation energy of YSZ was around  $0.87\text{ eV}$ , which was lower than the literature values. The activation energies decreased to unrealistic values for ionic conduction at temperatures above  $700^\circ\text{C}$ . Here electronic contributions might have played a part. Also the ionic conductivities were at least one order of magnitude lower than expected, this was attributed to electrode segregation. The YSZ film on STO had the highest conductivity throughout the whole temperature range, which can be caused by the difference in crystallinity. Though before drawing hard conclusions the measurements should be repeated. So at this moment, no clear answer can be given on the question how the crystal structure of YSZ influences the ionic conductivity.

# Table of contents

<b>Introduction .....</b>	<b>4</b>
<b>1 Theory .....</b>	<b>5</b>
1.1 Oxygen transport.....	5
1.2 Yttria-stabilized zirconia.....	5
<b>2 Experimental methods.....</b>	<b>7</b>
2.1 Pulsed Laser Deposition.....	7
2.1.1 The apparatus.....	7
2.1.2 Sample preparation and deposition parameters .....	7
2.2 Structural and composition analysis techniques.....	8
2.3 Impedance Spectroscopy.....	8
2.3.1 Theory.....	9
2.3.2 Modelling with circuit elements .....	9
2.3.3 Analysis .....	10
2.3.4 4-points measurements .....	11
2.3.5 Measurements.....	11
<b>3 The measurement system .....</b>	<b>12</b>
3.1 Configurations.....	12
3.1.1 Experimental.....	12
3.1.2 Stack configuration.....	13
3.1.3 Top electrodes.....	13
3.1.4 Side electrodes.....	13
3.2 Materials: Electrodes.....	13
3.2.1 Strontium Ruthenate .....	13
3.2.2 Platinum and gold.....	14
3.3 Materials: Substrates.....	14
3.3.1 Strontium Titanate .....	14
3.3.2 Neodymium Gallate.....	14
3.4 Wiring .....	15
3.5 Sample-holder .....	15
<b>4 Bonding wires and electrodes.....</b>	<b>16</b>
4.1 Wiring .....	16
4.1.1 Aluminium with 1% silicon.....	16
4.1.2 Gold .....	17
4.1.3 Other wiring.....	18
4.1.4 Conclusions .....	18
4.2 Electrodes.....	19
4.2.1 Results: SRO film.....	19
4.2.2 Results: Au film.....	20
4.2.3 Results: Pt film .....	21
4.2.4 Results: Pt-paste.....	21
4.2.5 Discussion and conclusions .....	22
4.3 Impedance measurements on a SRO electrode .....	22

<b>5</b>	<b>YSZ: structure and composition.....</b>	<b>24</b>
5.1	Deposition parameters.....	24
5.1.1	Experimental.....	24
5.1.2	Results .....	25
5.2	TEM .....	26
5.3	XPS .....	27
5.4	Discussion and conclusions.....	27
<b>6</b>	<b>YSZ: ionic conductivity .....</b>	<b>28</b>
6.1	Impedance measurements with the Al-1%Si wire .....	28
6.1.1	Stacks.....	28
6.1.2	Side electrode configuration .....	28
6.1.3	YSZ single crystals; instability in time.....	29
6.1.4	Nitrogen/oxygen influence .....	30
6.1.5	Discussion and conclusion.....	31
6.2	Impedance measurements with the Au wire .....	31
6.2.1	Reference samples .....	31
6.2.2	Single crystalline YSZ measurements .....	32
6.2.3	Thin YSZ films on NdGaO <sub>3</sub> and SrTiO <sub>3</sub> .....	34
<b>7</b>	<b>Discussion, conclusions and recommendations .....</b>	<b>37</b>
7.1	Discussion and conclusions.....	37
7.2	Recommendations .....	38
	<b>Dankwoord.....</b>	<b>39</b>
	<b>Literature .....</b>	<b>40</b>
	<b>Appendix I: Geometry calculations for the top electrode configuration.....</b>	<b>42</b>

## Introduction

Environmental pollution is a major topic these days because the temperature on earth is slowly increasing and the ozone layer is getting thinner. This problem is mainly attributed to the exhaust of green house gasses produced by, for example, cars. Several gasses can be found in the car exhaust such as NO, NO<sub>2</sub>, HC, CO, SO<sub>2</sub> and CO<sub>2</sub>. These gasses attribute to environmental problems like acid rain, smog and formation of ozone. The governments are continuously decreasing emission limits, which require better gas sensors with lower detection limits and faster reaction times.

In this report the ionic conductivity of yttria-stabilized zirconia (YSZ) was researched. YSZ transports oxygen through its lattice and can, for example, be used for the detection of oxygen and, indirectly, for NO<sub>x</sub> gasses. By using thin films instead of bulk materials, the ionic conductivity might be improved. Substrates with different lattice parameters will be used to influence the YSZ structure during deposition and hence the ionic conductivity. For measurements on ionic conductivities impedance spectroscopy is used because it can distinguish between the different resistance contributions, like bulk, grain boundary and electrode resistances. The measurements will take place in temperatures up to 900°C to comply with the high temperature requirements of oxygen gas sensors in car exhausts.

Impedance measurements on thin films at these temperatures are a new research topic and require a thorough preparation. The materials used for the electrodes and wiring of the sample, the measurement set-up and the sample configuration play an important role in obtaining successful measurements. Part of this research will therefore be contributed to finding the optimal conditions for ionic conductivity measurements on YSZ thin films.

The main objective of this thesis is to determine the influence of the crystal structure on the oxygen conductivity of thin YSZ films produced by pulsed laser deposition. Thereby searching for the crystal structure with the highest ionic conductivity. In order to measure correctly, the experimental conditions are studied as well.

The first chapter describes a theoretical background on the measurement methods as well as on the YSZ. The next two chapters give information about the equipment and set-up of the measurements. Chapter 4 focuses on the electrodes and wiring that were used to measure the YSZ. In chapter 5 YSZ is characterised and in chapter 6 the ionic conductivity of YSZ is discussed. Chapter 7 contains a discussion, the conclusions and the recommendations.

# 1 Theory

Yttria-stabilized zirconia is often used in gas sensing techniques as electrolyte. It transports oxygen through its lattice and is chosen for its high ionic conductivity and chemical stability in oxidizing, high temperature environments. Also it is relatively cheap.

## 1.1 Oxygen transport

Transport of oxygen through YSZ can be described with the Wagner theory<sup>1</sup>:

$$j(\text{O}_2) = \frac{RT}{4^2 F^2 L} \sigma_a \ln \left( \frac{P_{\text{O}_2,1}}{P_{\text{O}_2,2}} \right) \quad (0.1)$$

Here  $j(\text{O}_2)$  is the oxygen flux ( $\text{mol}/\text{m}^2\text{s}$ ),  $R$  the gas constant,  $T$  the temperature,  $F$  the Faraday constant,  $L$  the thickness of the electrolyte (m) and  $P_{\text{O}_2,1}$  and  $P_{\text{O}_2,2}$  the oxygen partial pressures at both sides of the electrolyte. It is assumed that the oxygen flux is not limited by the surface exchange reaction, only by bulk diffusion.  $\sigma_a$  is the ambipolar conductivity given by:

$$\sigma_a = \frac{\sigma_i \sigma_{el}}{\sigma_i + \sigma_{el}} \quad (0.2)$$

$\sigma_i$  is the ionic conductivity and  $\sigma_{el}$  the electronic conductivity. The ionic conductivity can be calculated with:

$$\sigma_i = n_i q_i \mu_i \quad (0.3)$$

With  $q_i$  the charge,  $n_i$  the number density and  $\mu_i$  the mobility of the species.

## 1.2 Yttria-stabilized zirconia

YSZ is manufactured by doping  $\text{ZrO}_2$  with the acceptor  $\text{Y}_2\text{O}_3$ . Zirconia exists in three phases, monoclinic up to  $1100^\circ\text{C}$ , tetragonal with distorted fluorite structure up to  $2400^\circ\text{C}$  and a cubic fluorite structure ( $\text{Fm}\bar{3}\text{m}$ ) above  $2400^\circ\text{C}^2$ . The cubic fluorite structure has a face-centered cubic (fcc) zirconia lattice and a cubic oxygen lattice placed in the fcc lattice. The  $\text{Zr}^{4+}$  cations occupy the tetrahedral sites and the  $\text{O}^{2-}$  anions the octahedral sites. The remaining octahedral sites are occupied by the  $\text{Zr}^{4+}$  cations, see Figure 1.1.

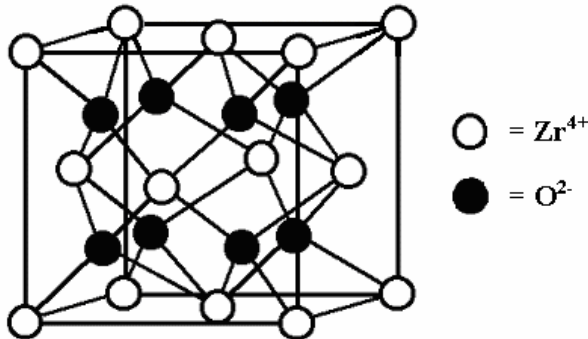


Figure 1.1: The cubic fluorite structure of  $\text{ZrO}_2$

The ionic conductivity of stabilized zirconia depends on the dopant concentration and the size of the acceptors. A minimum activation energy is found for acceptors with an ionic radius that closely matches that of the  $Zr^{4+}$  ion, of which  $Y^{3+}$  is one<sup>3</sup>. The addition of  $Y_2O_3$  stabilizes the zirconia cubic fluorite structure to room temperature and changes the non-conducting zirconia into an ion conducting material.

When doping  $ZrO_2$  with  $Y_2O_3$ , the  $Zr^{4+}$  cations in the  $ZrO_2$  lattice are substituted by the  $Y^{3+}$  cations thereby forming oxygen vacancies to maintain charge neutrality in the lattice. The oxygen vacancies make it possible for oxygen ions to move through the electrolyte by hopping from vacancy to vacancy in the lattice.

The defect reaction in Kroger-Vink notation<sup>4</sup>:



The oxygen vacancies are mobile at high temperatures and give rise to high oxygen ionic conductivity. More than 99% of the current through YSZ is carried by oxide ions. The oxygen vacancies experience two types of interactions in the lattice, the repulsion between the oxygen vacancies themselves and other positively charged carriers, and the attraction between oxygen vacancies and the acceptor  $Y$ <sup>5</sup>.

The maximum ionic conductivity lies around 8-9 mol%  $Y_2O_3$  doping. At higher doping the attraction between the oxygen vacancies and the yttria will result in the formation of complexes and decreases the mobility of the oxygen vacancies. The complex has a positive effective charge when an oxygen vacancy is bonded to only one cation<sup>6</sup>:



A further increase of the yttria concentration, and thereby the vacancy concentration, gives more complex associations, which can form clusters. In these clusters the oxygen vacancy is bonded to two cations, decreasing the oxygen vacancies' mobility further. This complex is electrostatically neutral<sup>6</sup>:



Besides a good ionic conductivity, YSZ exhibits a high micro hardness, is corrosion resistant, has a low thermal conductivity and is chemically stable at high temperatures<sup>2</sup>.

## 2 Experimental methods

This chapter describes the methods that were used to produce and characterise the samples.

### 2.1 Pulsed Laser Deposition

Pulsed laser deposition (PLD) is a thin film deposition technique; key features are a broad useable pressure range, stoichiometric transfer from the target to the film and a high deposition rate.

#### 2.1.1 The apparatus

The laser used was a Lambda Physik KrF excimer laser with  $\lambda = 248$  nm and a pulse duration of about 20-30 ns. The focused laser beam ablates material from the target and produces a plasma plume with ablated material (Figure 2.1). The fluency (together with the spot size it gives the energy density of the laser on the target) mainly determines the amount of ablated material and determines if stoichiometric ablation takes place. The kinetic energy of the particles depends on the gas pressure as well as on the substrate temperature. At high gas pressure, the ablated species will accelerate mainly in the direction of the substrate (narrow visible plume); a low pressure results in a broad visible plume. During the transfer from the target to the substrate the ablated species will interact with each other and with the gas molecules in the chamber. Therefore the target-to-substrate distance and the gas pressure in the chamber are very important parameters. When the ablated material reaches the substrate it will be adsorbed on the substrate and a thin film is grown.

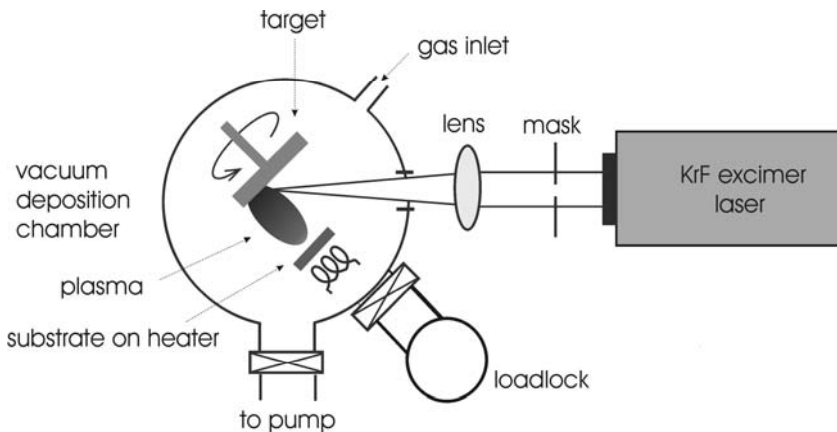


Figure 2.1: PLD system

Important parameters during deposition are the substrate temperature, the gas pressure, the energy density on the target and the target-to-substrate distance.

#### 2.1.2 Sample preparation and deposition parameters

The thin films were deposited on substrates with the dimensions of  $5 \times 5 \times 0.5$  mm<sup>3</sup>. The most used substrate was SrTiO<sub>3</sub> (STO) because it is very suitable to grow epitaxial SrRuO<sub>3</sub> (SRO) and YSZ films on. The TiO<sub>2</sub> terminated STO substrates were treated directly before the deposition to remove any contamination:

- 15 minutes ultrasonic cleaning in high quality acetone
- 15 minutes ultrasonic cleaning in high quality ethanol
- Mechanical cleaning with lens tissues
- 10 minutes ultrasonic cleaning in high quality ethanol

In the case of multi-layered films the depositions were done *in situ*, meaning that all layers were deposited without removing the sample from the vacuum chamber. This decreased the chance on contamination considerably.

The deposition parameters can be found in Table 2.1.

**Table 2.1: Pulsed laser deposition parameters**

	<b>8-YSZ</b>	<b>SRO</b>	<b>Pt</b>
Laser energy density [J/cm <sup>2</sup> ]	2.1	2.5	4.0
Spot size [mm <sup>2</sup> ]	3.36	1.94	3.00
Pressure [gas; mbar]	O <sub>2</sub> ; 2.1·10 <sup>-2</sup> -2·10 <sup>-4</sup>	O <sub>2</sub> ; 0.13	Ar; 0.25
Substrate Temperature [°C]	600-900	600	23
Laser frequency [Hz]	7	2 or 6	10
Target-to-substrate distance [mm]	59	49	48
Deposition rate [Å/pulse]	0.26	0.12	unknown

The deposition rates of YSZ and SRO were determined by measuring the thickness of a deposited film with low angle-XRD.

## 2.2 Structural and composition analysis techniques

The structure of YSZ plays an important role in ionic conductivity measurements. Several techniques were therefore used to study the YSZ structure, its composition and the morphology. Some techniques were also used to examine the electrodes. A short overview of the techniques is given below.

Atomic force microscopy (AFM) was used for the determination of the surface morphologies, the inspection of a surface for contaminations (Figure 2.2a/b) and determination of the growth behaviour of YSZ on STO (Figure 2.2c). The measurements were done with a Nanoscope 4 multimode AFM from Digital Instruments.

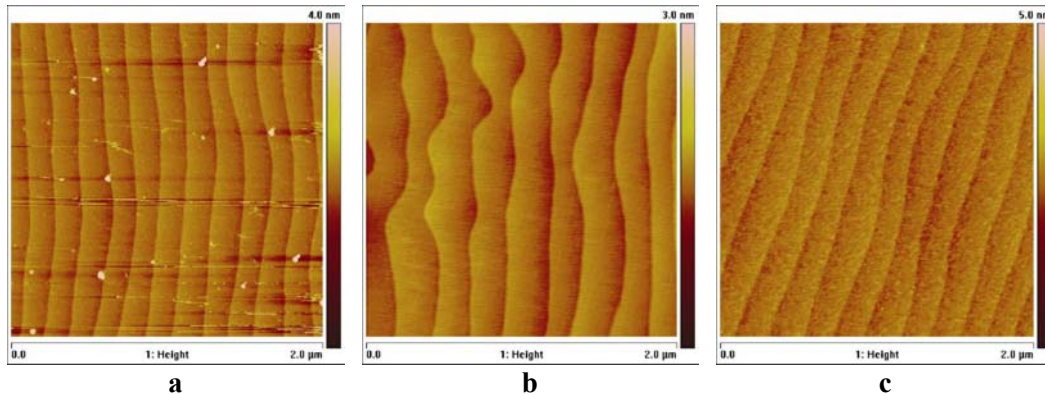


**Figure 2.2: AFM images of a) STO substrate with contaminations; b) STO substrate without contaminations after mechanical cleaning; c) 30 nm YSZ film deposited on STO, the step edges are still visible, indicating smooth growth of YSZ on STO**

X-ray diffraction (XRD) was used to determine the film crystallinity and low-angle XRD was used to determine the film thickness (and hence the deposition rate). For the measurements an Enraf-Nonius Delft CAD4 diffractometer was used. X-ray photoelectron spectroscopy (XPS) was used to measure the composition of the deposited films. With a transmission electron microscope (TEM) the crystallinity, as well as the surface morphology were studied. Scanning electron microscopy (SEM) was used to study the morphology when a surface was too rough to study with AFM.

## 2.3 Impedance Spectroscopy

For measurements on ionic conductivities impedance spectroscopy was used because it can distinguish between the different resistance contributions, like bulk, grain boundary and electrode resistances. It is a useful technique when researching the measurement conditions and the influence of the YSZ structure on the ionic conductivity.

### 2.3.1 Theory

The impedance is measured by applying a small AC potential to the sample with varying frequencies. The current response is measured. The phase shift and amplitude of the response signal give information about the impedance<sup>7</sup>.

$$Z(\omega) = \frac{V(\omega)}{I(\omega)} = \frac{V_0 \sin(\omega t)}{I_0 \sin(\omega t + \varphi)} \quad (1.1)$$

In this equation,  $Z$  is the impedance,  $V$  the voltage,  $I$  the current,  $\omega$  the radial frequency ( $2\pi f$ ),  $j$  the imaginary unit and  $\varphi$  the phase shift.

With Eulers relationship ( $\exp(j\varphi) = \cos \varphi + j \sin \varphi$ ), relationship (1.1) can be expressed as a complex number:

$$Z(\omega) = \frac{V_0 e^{j\omega t}}{I_0 e^{j(\omega t - \varphi)}} = Z_0 (\cos \varphi + j \sin \varphi) \quad (1.2)$$

The real part is the resistance and the imaginary part is composed of the inductive reactance and capacitive reactance. In a graphical representation the real part ( $Z_0 \cos \varphi$ ) is plotted versus the imaginary part ( $Z_0 j \sin \varphi$ ), see Figure 2.3.

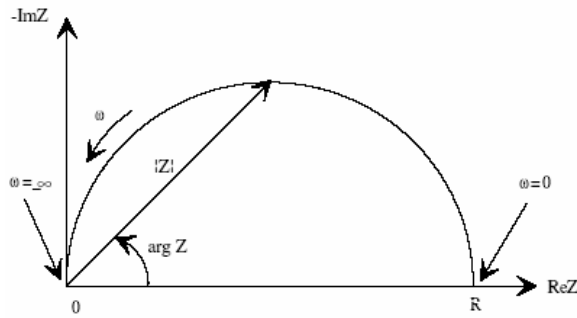


**Figure 2.3: Nyquist plot with impedance vector; the impedance is represented as a vector of length  $|Z|$ , the angle between this vector and the x-axis is  $\varphi$  ( $=\arg Z$ );  $\omega$  is the angular speed,  $\text{Re}Z$  the real impedance part and  $\text{Im}Z$  the imaginary impedance part.**

### 2.3.2 Modelling with circuit elements

The impedance spectroscopic data is commonly analysed by fitting it to an equivalent circuit model. This model can consist of several circuit elements like resistors, capacitors, constant phase elements (CPE) etc. The modelling of data with circuit elements provides a physical meaning to the impedance data. The circuit elements are listed in Table 2.1.

**Table 2.1: Circuit elements used in models**

Equivalent element	Description	Impedance	Admittance
R	Resistance	R	$1/R$
C	Capacitor	$1/j\omega C$	$j\omega C$
L	Inductance	$j\omega L$	$1/j\omega L$
W	Warburg (semi-infinite diffusion)	$1/Y_0 \sqrt{j\omega}$	$Y_0 \sqrt{j\omega}$
Q	CPE (constant phase element) $\alpha = -1 \Rightarrow$ CPE = inductance $\alpha = 0 \Rightarrow$ CPE = resistance $\alpha = 0.5 \Rightarrow$ CPE = Warburg $\alpha = 1 \Rightarrow$ CPE = capacitor	$1/Y_0 (j\omega)^\alpha$	$Y_0 (j\omega)^\alpha$

Fitting the measurement data was done with the software EQUIVCRT.

### 2.3.3 Analysis

The conductivity of a sample can be calculated when the resistance is measured and the geometry is known:

$$\sigma = \frac{d}{RA} \quad (1.3)$$

With  $R$  the resistance ( $\Omega$ ),  $d$  the distance between the electrodes (m),  $A$  the electrode surface ( $m^2$ ) and  $\sigma$  the conductivity (S/m).

The impedance spectroscopic data are used to calculate the activation energy and the conductivity by plotting  $\ln(\sigma T)$  versus  $1/T$  from equation (1.4).

$$\ln(\sigma T) = \ln \sigma_0 + \frac{-E_{\text{act}}}{R} \cdot \frac{1}{T} \quad (1.4)$$

With  $E_{\text{act}}$  the activation energy (J/mol) and  $R$  the gas constant.

From the slope of the trend line the activation energy is calculated. The activation energy gives information about the amount of free vacancies and the mobility of these vacancies. At low temperatures the activation energy is used to free vacancies from complexes and for the mobility of the vacancies. At higher temperatures, when complexes no longer hold the vacancies, the activation energy is only used for mobility and can therefore be lower than at low temperatures.

There are two possibilities to fit the data in the Arrhenius plots (Figure 2.4). First, a fit with a straight line. This was used to calculate the activation energy over a temperature range. The intercept at the y-axis gives the  $\sigma_0$  of the sample.

In the second case, when the data was fit with a second order polynomial, the activation energies and ionic conductivities could be calculated at each temperature individually.

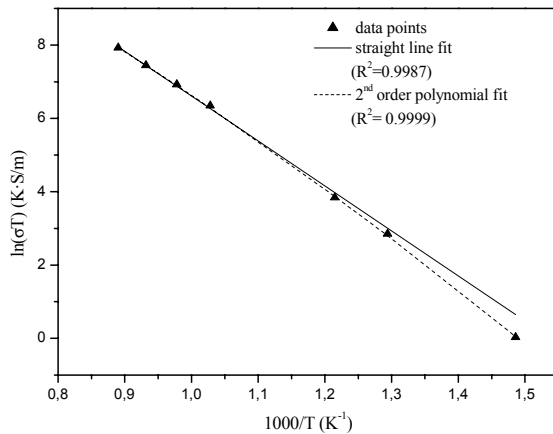


**Figure 2.4: Arrhenius plots to calculate the activation energy. The first three points (850°C- 800°C-750°C) lie in a straight line. The more the temperature decreases, the larger the deviation from the straight line is.**

In the case of YSZ the best fit was usually obtained with a second order polynomial function, because at higher temperatures the activation energy became lower. Though for comparison with literature values or when the data did not fit a second order polynomial function, straight lines were used to fit the data, in most cases one for the low temperature range (~400-600°C) and one for the high temperature range (~700-900°C).

### 2.3.4 4-points measurements

4-points measurements (van der Pauw) have been considered because this method eliminates the geometrical factor. With this method an A/C current is sent through the electrolyte while the voltage is measured just before the electrodes (Figure 2.5). Unfortunately in the case of ionic conductivity there is no continuous flow into the electrodes like in the case of electrical conductivity. Instead the A/C current moves the oxygen to the outer electrodes. Therefore, the inner electrodes are not able to measure the voltage and 4-point measurements are not an option in the oxygen conductivity measurements.

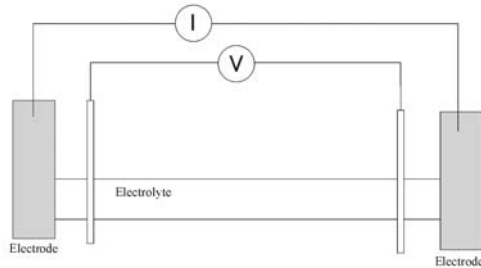


Figure 2.5: Set-up 4-point measurements; view from above

### 2.3.5 Measurements

The measurements were done in the range of 1-65535 Hz, with a Solartron Schlumberger 1250 Frequency Response Analyser. The temperature varied between 23 and 900°C. Nitrogen or oxygen gas was applied to the system.

### 3 The measurement system

For measurements on a thin film system with two electrodes and an electrolyte a special sample design was required. The impedance measurement system was adapted to the small samples, including the wiring. The high temperatures and oxygen environment increased the standards for the electrodes, wiring and sample-holder. All parts had to be able to withstand these circumstances.

#### 3.1 Configurations

The sample configuration is very important. Two to three different materials have to be deposited on the same substrate in different geometric forms. Preferentially, this should be done *in situ*, without removing the sample from the vacuum chamber to avoid contamination. For the conductivity calculations it is required that the geometry of the sample, the electrode surface and the distance between the electrodes, is known. The three configurations used in this research are schematically shown in Figure 3.1, Figure 3.2 and Figure 3.3. The next paragraphs give information about the configurations.

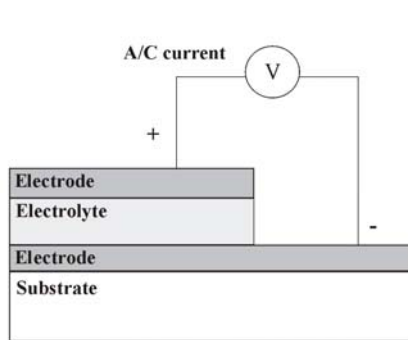


Figure 3.1: Schematic overview of a stack configuration

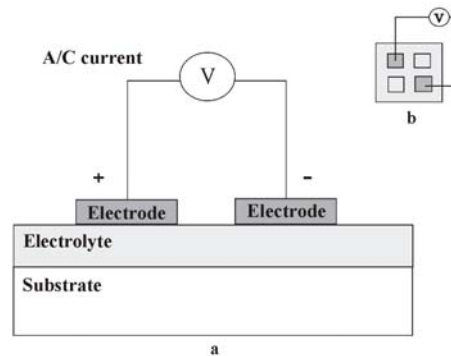


Figure 3.2: Schematic overview of a sample with top electrodes; a is the side view, b is from above

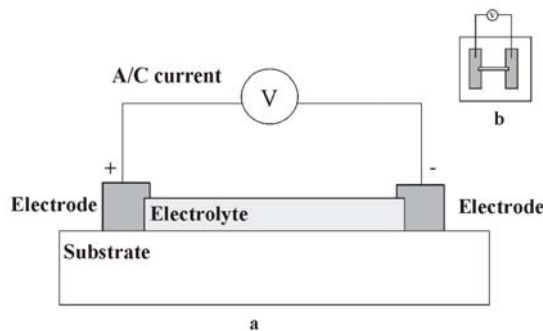


Figure 3.3: Schematic overview of a sample with side electrodes; a is the side view, b is from above

##### 3.1.1 Experimental

The configurations were formed by etching part of the deposited films, using a photoresist film as mask. Two etching techniques were considered and tested. First  $\text{Ar}^+$  etching, which is suitable to etch SRO as well as YSZ and was therefore the preferred method. However, during  $\text{Ar}^+$  etching there was the possibility that the removed particles redeposit on the SRO film and/or on the side of the YSZ and SRO film. In the worst case, redeposition of SRO on the YSZ side could cause a short circuit between the SRO electrodes. The second method was chemical etching with buffered-HF (BHF) which can only etch YSZ, but reassured that there was no contact between the SRO electrodes because the sides of the YSZ film were etched in.

The etch rates of both methods were determined by low-angle XRD measurements. Unfortunately, the etch rate of BHF could not be determined accurately and was therefore not suitable for precise etching. Instead, Ar<sup>+</sup> etching was used. To check if the sample short-circuited, the resistance was measured before the impedance measurements. A low resistance indicates a possible short-circuited system.

After the sample was etched, two Al-1%Si<sup>a</sup> or Au wires were bonded to the electrodes to make contact with the (thicker) Pt wires of the measuring system.

### 3.1.2 Stack configuration

With pulsed laser deposition samples were made in the stack configuration. The stack consisted of SRO and YSZ films on STO in the following sequence: SRO-YSZ-SRO. Part of the SRO and YSZ films were etched and connections were made to both SRO electrodes.

### 3.1.3 Top electrodes

The configuration with top electrodes was the simplest to produce, consisting of only three steps. The first step was the deposition of the YSZ film on the substrate, second the deposition of the electrode film on top of YSZ. Finally, with Ar<sup>+</sup> etching part of the electrode film was removed and four electrodes of 1 x 1 mm<sup>2</sup> were formed. Two electrodes were connected and used for impedance measurements.

The shape and orientation of the electrodes caused difficulties in determining the pathway of the oxygen diffusion. The geometry calculations can be found in Appendix I.

### 3.1.4 Side electrodes

A configuration with a defined geometry (electrodes on each side of the electrolyte, in plane) was chosen to replace the stack configuration. The configuration was composed in two steps. First a YSZ film was deposited after which the structure was etched in the film. In the second step a photoresist mask was applied to the sample through which the electrode was deposited. This configuration had a better-defined geometry compared to the configuration with the top electrodes. The electrodes surface was calculated by multiplying the thickness of the YSZ film with the width of the film. The small overlapping part of the electrode on the YSZ film was negligible compared to the length of the YSZ film.

## 3.2 **Materials: Electrodes**

To measure the ionic conductivity of YSZ, electrical conducting electrodes were needed that were porous enough to ensure oxygen transport through the electrode to YSZ. The YSZ and electrode material should have similar lattice parameters to ensure epitaxial growth of the films. 8-YSZ has a cubic lattice constant of 5.139 Å. The electrodes also needed to remain chemically stable at high temperatures in an oxygen environment

In literature the most common substrates used for YSZ deposition are Si(001) and sapphire(001). But both are not suitable as electrode materials because silicon oxidizes very quickly and sapphire (Al<sub>2</sub>O<sub>3</sub>) is not electrical conducting. Though sapphire could be used as substrate for the deposition of thin films. Other electrode materials were found and are discussed in the next paragraphs.

### 3.2.1 Strontium Ruthenate

SrRuO<sub>3</sub> is a good conducting metallic oxide and chemically very stable up to temperatures of 1200K<sup>8</sup>. It can be grown epitaxially on the substrate STO that has comparable lattice parameters and is porous towards oxygen. No deposition data of YSZ on SRO grown by PLD was found in literature.

---

<sup>a</sup> Aluminum with 1% silicon; the silicon is added to make the aluminum ductile

The epitaxial growth of YSZ on SRO is possible by a 45° rotation in plane by the unit cell of YSZ (Figure 3.4). The misfit between YSZ and SRO (pseudo cubic lattice constant 3.924 Å) is ~7.2 %.

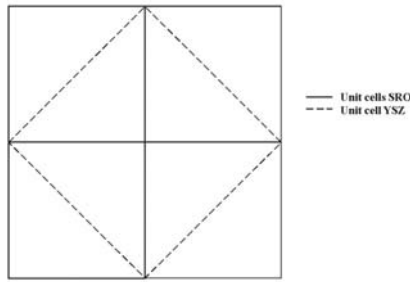


**Figure 3.4: 45° in plane rotation of unit cell YSZ on unit cells SRO**

### 3.2.2 Platinum and gold

Platinum and gold are noble metals with melting temperatures of 1772°C and 1064°C<sup>10</sup>, respectively. Both materials were used as electrodes and gold also as wiring.

## 3.3 Materials: Substrates

A substrate which is suitable to use in ionic conductivity measurements for thin films should not influence the total resistance. In the top electrode configuration the current flow is parallel to the substrate surface, involving film, interfacial and substrate contributions. However, when the resistance of the substrate is much higher than of the film and interface, the total resistance is only determined by the film and/or interface<sup>3</sup>. Therefore, the substrate should be an ionic insulator. It should also be a material on which the films (for example YSZ) can be deposited epitaxially.

### 3.3.1 Strontium Titanate

SrTiO<sub>3</sub> is an insulator and suitable to use as substrate for the deposition of thin films. The substrate was oriented in the [001] direction. STO is extremely suitable for deposition of SRO because the lattice parameters are very similar.

### 3.3.2 Neodymium Gallate

NdGaO<sub>3</sub> (NGO) has a pseudo cubic structure in its orthorhombic structure. NGO has different lattice parameters than STO and was therefore used to change the structure of YSZ. The substrate was oriented in the [001] direction.

Table 3.1 gives an overview of all the materials properties.

**Table 3.1: Materials properties overview**

	Electrolyte		Electrodes		Substrates	
	YSZ-8	SRO <sup>8</sup>	Pt	Au	STO <sup>8</sup>	NGO
Structure	cubic	orthorhombic perovskite (pseudo cubic)	cubic	cubic	cubic	orthorhombic
Lattice constants [Å]	5.139	a = 5.573 b = 7.856 c = 5.538 (3.924)	3.920	4.08	3.905	a = 5.418 b = 5.496 c = 7.693
Di-electric constant $\epsilon_r$ [-]	25	-	-	6.9 <sup>9</sup>	277	20 <sup>11</sup>
Melting Point [°C]	2710 <sup>b</sup>	-	1772 <sup>10</sup>	1064 <sup>10</sup>	2080 <sup>11</sup>	1600 <sup>11</sup>

<sup>b</sup> for 10-15 mol% YSZ

### 3.4 Wiring

The deposited electrodes were connected to the system with thin wires (diameter 25 $\mu$ m) that were ultrasonically bonded to the film. Two types of wires were used, an aluminium wire with 1% silicon and a gold wire.

### 3.5 Sample-holder

The sample-holder was especially designed for measurements in thin films. The sample-holder supported the transition from the thin bonding wires on the sample to larger Pt wires that were connected to the frequency response analyser (FRA). The sample-holder was surrounded by a quartz tube flushed with oxygen or nitrogen gas and shoved in a platinum tube in the oven. The platinum tube shielded the system from unwanted frequencies from outside. The temperatures were set with an Eurotherm 815 and had a maximum deviation of  $\pm 0.3^{\circ}\text{C}$  during measurements, measured with a S-type thermocouple situated in close proximity to the sample.

In the first prototype the platinum wires of the sample-holder and the system were connected using wiring block terminals (consisting of Ti blocks with Pt screws). However these screws were not resistant to a temperature of 900 $^{\circ}\text{C}$  in oxygen. Under these circumstances the screws oxidized to such an extent that it was impossible to remove the wires and often the screws broke. In the new design the screws were left out, the wires were welded together instead.

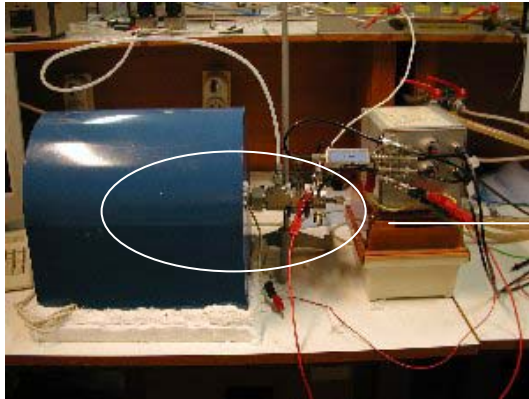


Figure 3.5: Impedance measurements set up; on the left the blue oven containing the sample holder; on the right the measurement equipment



Figure 3.6: The sample-holder as it is shoved into the oven

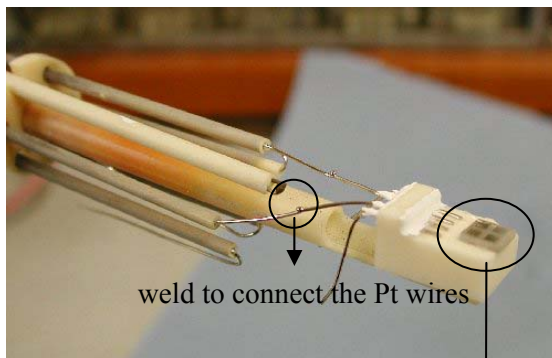


Figure 3.7: Detail of the sample-holder with sample

sample 5x5x0.5mm<sup>3</sup>

## 4 Bonding wires and electrodes

Bonding wires and electrodes are an important part of the measurement set-up. The bonding wires need to ensure a good connection between the electrodes and the measurement system. The electrodes should transport oxygen to the electrolyte, be electrical conductive and remain stable throughout the measurements.

The thin YSZ films can only be measured correctly when bonding wires and electrodes are constant factors and their contribution to the resistance is negligible. Therefore, both were studied on their behaviour at high temperatures in an oxygen environment.

### 4.1 Wiring

The two types of wires that were used are discussed in the next paragraphs.

#### 4.1.1 Aluminium with 1% silicon

The Al-1%Si wire is often used in the semi-conductor industry as bonding wire because of its strength, flexibility and conductivity. The bonding of the wire to thin films was easily carried out, but when the impedance measurements of the samples gave very high resistances, the wire and its bond were examined more closely at their behaviour at higher temperatures in an oxygen environment.

The Al-1%Si wire was tested for its stability in time at constant temperature and at different temperatures. Measurements at different temperatures in an oxygen environment demonstrated that the wire and its bond had a low resistance around 1 Ohm. But at high temperatures  $> 580^{\circ}\text{C}$ , the resistance of the wire and/or bond increased dramatically to the order of kOhms (Figure 4.1).

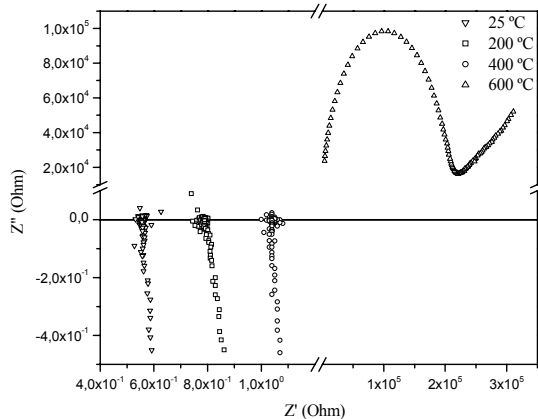


Figure 4.1: Impedance measurement of the Al-1%Si wire at different temperatures

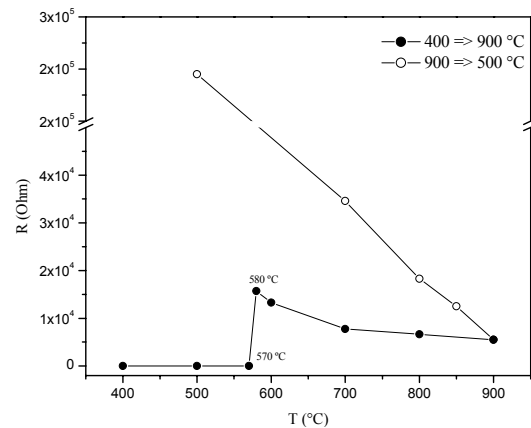


Figure 4.2: Resistance at different temperatures

At 25, 200 and  $400^{\circ}\text{C}$  the impedance graphs show the self-induction of the Al-1%Si wire, which is close to zero if the resistance of the system was subtracted ( $\sim 0.5$  Ohm). At  $580^{\circ}\text{C}$  the resistance suddenly increased. At this point the wire was not yet broken because when the wire was broken the resistance was indefinitely high and no semi-circles were observed.

Increasing the temperature to  $900^{\circ}\text{C}$  lowered the resistance of the wire but did not meet any trend (Figure 4.2). During cooling down the resistance increased again indicating an irreversible change. The sudden increase in resistance at  $580^{\circ}\text{C}$  was caused by deformation of the bond and/or wire. The Al-Si phase diagram (Figure 4.3) shows a phase change for 1%Si in Al, between  $574$ - $615^{\circ}\text{C}$ .

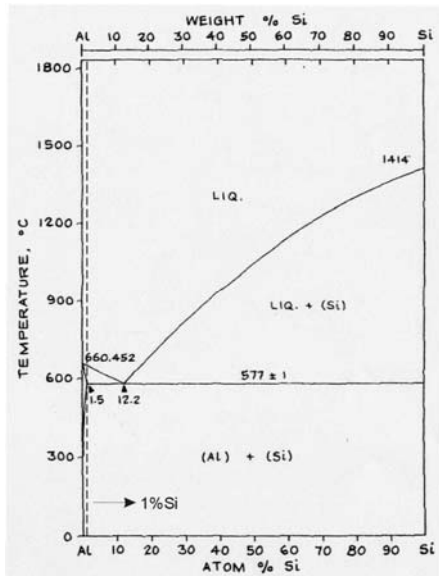


Figure 4.3: Al-Si phase diagram; 1% Si is marked with a dotted line<sup>12</sup>

In this temperature range a liquid Al phase is formed, which can easily deform the wire. Also oxidation was a problem as can be derived from the increasing resistance while cooling down. Oxidation has the most influence on the bond because the bond is relatively thin compared to the wire and should maintain a good contact with the surface of the electrode to keep contact-resistance low (the resistance is inversely proportional to the contact area). Figure 4.4 shows the ‘before’ and ‘after’ pictures of the Al-1%Si wire and it can be seen that the wires looked very fragile after the measurements.

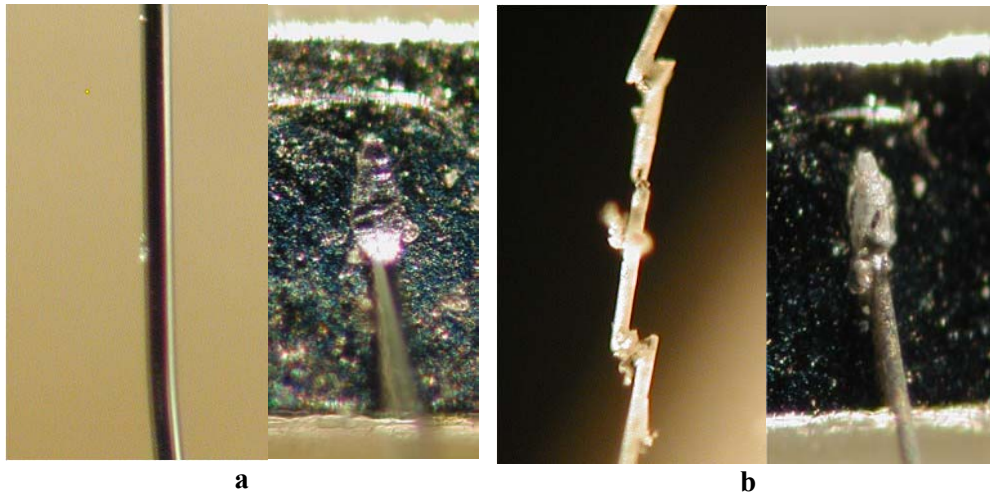


Figure 4.4: Al-1%Si wire and bond; a) before measurements; b) after measurements at 900 °C in oxygen environment

It can be concluded that the Al-1%Si wire is not suitable for measurements above 580°C in an oxygen environment

#### 4.1.2 Gold

As a replacement for the Al-1%Si wire, gold was chosen. The melting point of gold was sufficiently above the highest measuring temperature of 900°C and this noble metal will not easily oxidize.

The Au wire was measured in the same way as the Al-1%Si wire. The resistance of the gold wire remained low up to a temperature of 930°C. Cooling down fast to 800°C resulted in a high resistance indicating that the wire and/or bond underwent irreversible changes which could be due to stress that occurred due to the fast cooling temperature. The experiment was

repeated by cooling down with a rate of  $1^{\circ}\text{C}/\text{min}$  and no sudden increase in resistance was found during the first  $200^{\circ}\text{C}$  of the cooling. In a third experiment the gold bond remained stable after heating up and cooling down several times from room temperature to  $900^{\circ}\text{C}$ . This indicates that an important factor is the strength of the bond. To attach the gold wire to the very thin films a larger force had to be used than with the Al-1%Si wire which could damage the film or even push the wire through the film. To facilitate the bonding, the substrate was heated to  $100\text{-}150^{\circ}\text{C}$ , though bonding remained difficult. Each time the same parameters were used for bonding the wire, but the rough surface of the Pt wire can have influenced the final strength of the bond. Also the contact area of the bond could be different. Despite all, the gold wire seemed a good alternative for the Al-1%Si wire. However, the strength of the gold bond was not known on thin SRO and Pt films.

The resistance of an Au bonding wire was also tested at constant temperature to determine the stability over a period of time. The resistance of the bonding wire was directly constant around  $1.2\ \text{Ohm}$  and remained constant for more than 16 hours. After 16 hours the resistance became instable and increased a little until, after 21 hours, the resistance increased enormously to a resistance of  $37\ \text{kOhm}$  and stayed there, slightly increasing in time (Figure 4.5). The mobility of Au probably plays a part in this increase because it could be seen that after long annealing the bond started to segregate slowly. Also the relaxation of stress, occurred during the bonding process, could have attributed to the increase.

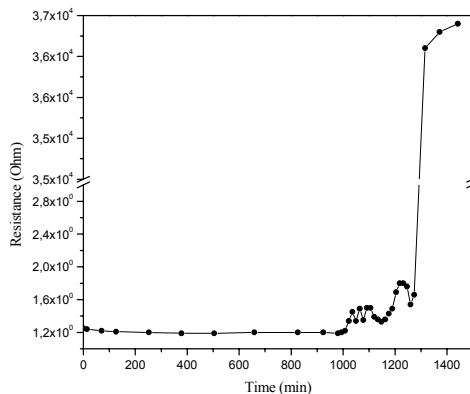


**Figure 4.5: Resistance of an Au bonding wire in time at  $700^{\circ}\text{C}$  in oxygen environment**

From this experiment it was concluded that the Au wire remains stable enough to measure in the required circumstances.

#### 4.1.3 Other wiring

Other wire materials that can be considered are palladium (Pd) and platinum (Pt). These materials have high melting points ( $1552^{\circ}\text{C}$  and  $1772^{\circ}\text{C}^{10}$ , respectively), but are more expensive and require higher bonding energies complicating the bonding process. However, platinum would be an interesting alternative because platinum was also used for the thicker wires to connect the thin bonding wires with the system.

#### 4.1.4 Conclusions

The Al-1%Si wire is not suitable for measurements above  $580^{\circ}\text{C}$  in an oxygen environment. The gold wire seems a good alternative. It remained stable up to high temperatures over a sufficiently long time. However, the strength of the gold bond is not known on thin SRO and Pt films.

## 4.2 Electrodes

Four materials were tested on their suitability to serve as electrodes for YSZ, see Table 4.1.

**Table 4.1: The four electrode samples**

Sample name	Substrate	Film	Film thickness [nm]	Remarks
YSZ <sub>sc</sub> -SRO	YSZ <sub>sc</sub> <sup>c</sup>	SRO	100	Deposition parameters in Table 2.1
YSZ <sub>sc</sub> -Au	YSZ <sub>sc</sub>	Au	± 100	T <sub>deposition</sub> 23°C, fluency 5 J/cm <sup>2</sup> , spotsize 2.16 mm <sup>2</sup> , d <sub>target,substrate</sub> 53 mm, frequency 5 Hz; deposition rate guessed
YSZ <sub>sc</sub> -Pt	YSZ <sub>sc</sub>	Pt	± 100	Deposition parameters in Table 2.1
YSZ <sub>sc</sub> -Pt-paste	YSZ <sub>sc</sub>	Pt-paste	Unknown	Fabricant: Compoir Lyon-Alemand Louyot

The four samples were placed together in an oven and brought to the annealing temperature with a heat-up rate of 3°C/min. In the first annealing step the samples were heated up to 600°C and kept there for 5 hours. Thereafter, the samples were cooled down with 3°C/min and examined with AFM. The same samples were heated up again to 700°C and programmed to anneal for 5 hours. In the last annealing step the temperature was raised to 900°C at which the samples stayed for 5 hours<sup>d</sup>.

### 4.2.1 Results: SRO film

The SRO structure was clearly changing during annealing, see Figure 4.6. Starting with very small spherical particles with a height < 20 nm and a diameter < 125 nm, after heat treatment at 600°C the particles were higher than 125 nm and the diameter doubled. The particles also lost their spherical shape. This change in structure was remarkable because SRO was deposited at 600°C and therefore expected to be stable at least that temperature. The only difference was the oxygen pressure which was 0.13 mbar during deposition instead of ~200 mbar during annealing. An explanation might be the growth direction in which SRO was deposited. It was expected that SRO was chemically stable at high temperatures as reported in literature<sup>8,13</sup> when SRO was grown on STO. In that case the growth direction of SRO on STO was [001]SRO//[100]STO and [-110]SRO//[010]STO (orthorhombic frames). Though, Zhu et al.<sup>14</sup> reported a different growth of SRO on [100]YSZ described as the epitaxial relation [110]SRO//[100]YSZ and [-110]SRO//[011]YSZ. Here, the SRO grows with its pseudocubic [110]plane parallel to the substrate surface. The other orientation of SRO on YSZ might explain the instability at high temperatures compared to the SRO film deposited on STO because the morphology changes. During crystallization other facets can be formed that result in the observed structure (Figure 4.6d).

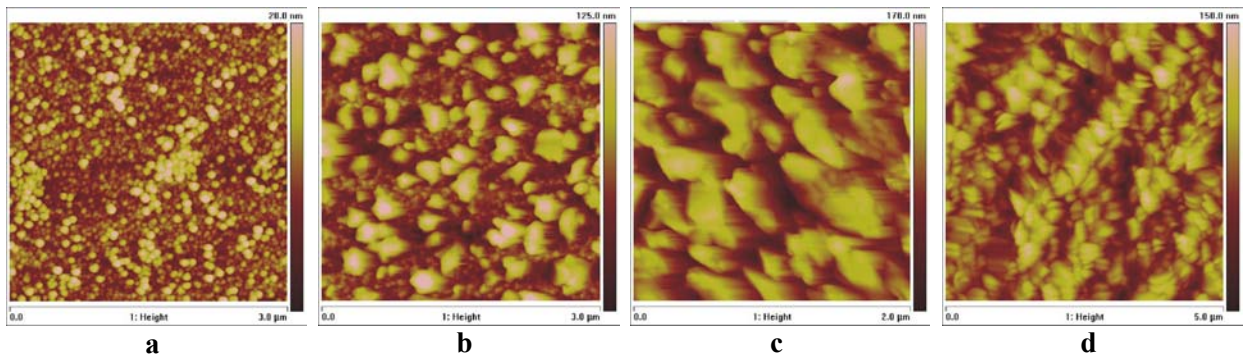


**Figure 4.6: AFM height images of YSZ<sub>sc</sub>-SRO; a) as deposited, b) after annealing at 600°C, c) after annealing at 700°C; d) after annealing at 900°C**

After annealing at 900°C the particles seemed to be completely segregated to larger structures with heights >150 nm. With an optical microscope a dispersed film with very fine particles was seen.

<sup>c</sup> sc = single crystal

<sup>d</sup> Instability of the oven caused some temperature fluctuations

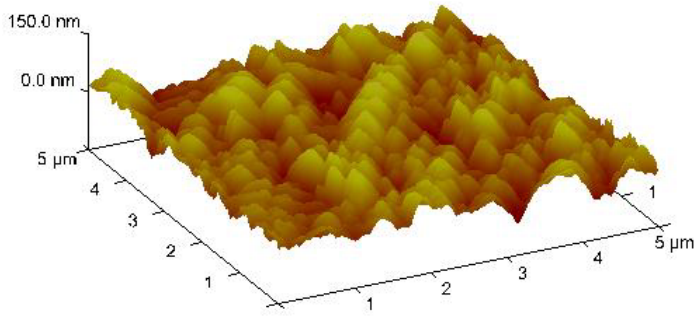


Figure 4.7: AFM 3D height image of YSZsc-SRO after annealing at 900 °C

A major difference was seen after impedance measurements at 900°C on a 200 nm SRO film on YSZ. This sample was annealed for two hours at 920°C in 0.13 mbar oxygen pressure before the measurements. The SRO film revealed a much more segregated structure which could be seen very clearly with the optical microscope.

#### 4.2.2 Results: Au film

The height profile of the Au films was changing less rapidly as it did in the case of the SRO film. At 700°C the height profile was still < 30 nm. Though after annealing at 900°C a gold network was visible (Figure 4.8d) with a height of approximately 1000 nm, five times higher than the final height of the SRO film. The network started to form before 600°C and was so porous that the YSZ substrate could be seen through the gold structures.

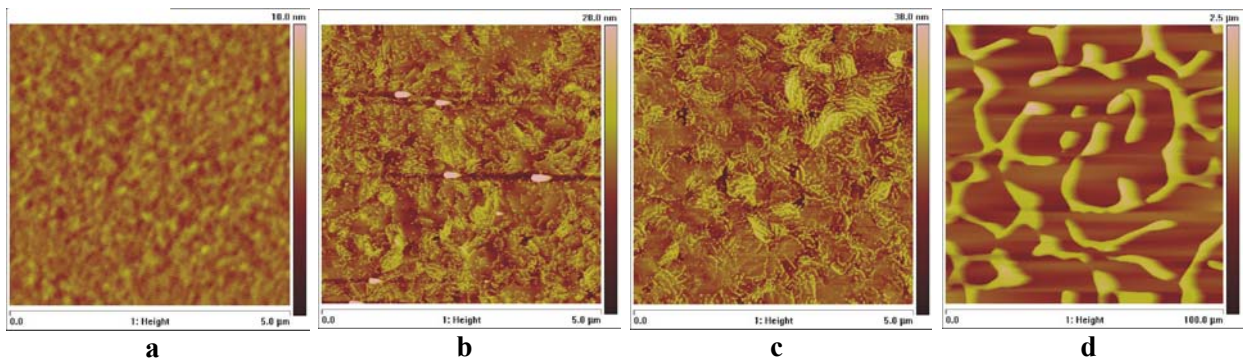


Figure 4.8: AFM height images of YSZsc-Au; a) as deposited, b) after annealing at 600°C, c) after annealing at 700°C; d) after annealing at 900°C

The network could also be seen with an optical microscope (enlargement 25x). The formation of these large structures makes the bond, connecting the wire and electrode, very weak. The contact area between the electrode and electrolyte is decreasing significantly and will cause an increase in contact-resistance.

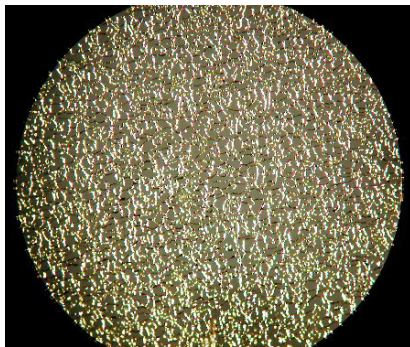


Figure 4.9: Optical microscope picture

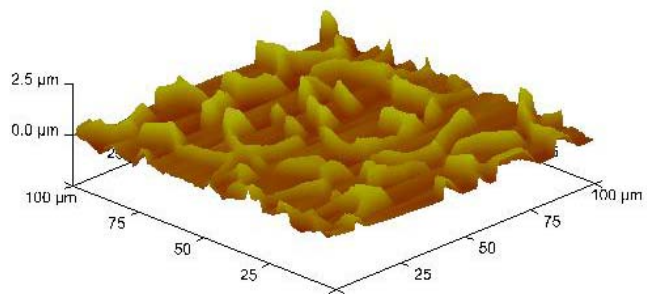
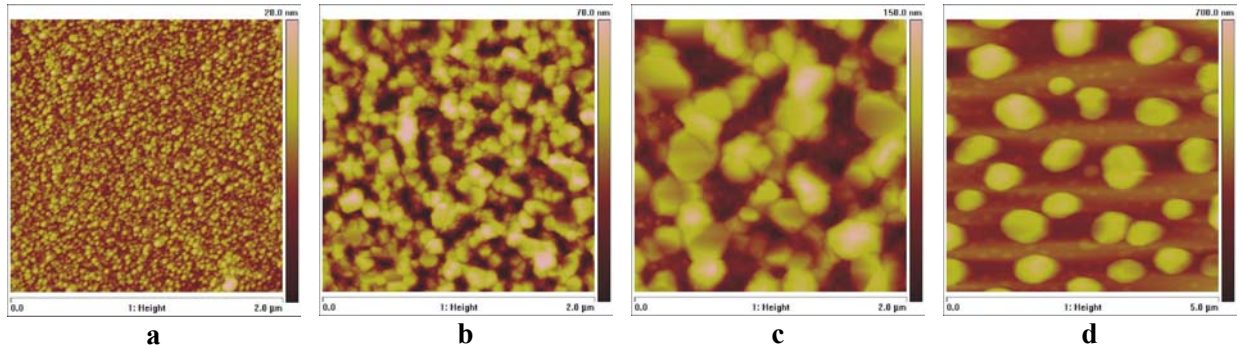


Figure 4.10: AFM 3D height image of YSZsc-Au after annealing at 900°C

In conclusion, a 100 nm gold electrode seems not applicable at temperatures up to 900°C because the film forms a very porous network, thereby increasing the contact-resistance.

#### 4.2.3 Results: Pt film

The platinum film also segregated to small islands with diameters that reached 800 nm and a height of > 700 nm (Figure 4.11d). The particles were dispersed over the whole surface. The contact area between the electrode and the bond decreased, leading to an increase in resistance. Also the strength of the bond was decreasing.



**Figure 4.11: AFM height images of YSZsc-Pt; a) as deposited, b) after annealing at 600°C, c) after annealing at 700°C; d) after annealing at 900°C**

A similar sample (YSZsc-Pt3) was annealed for 4 hours at 900°C in 0.25 mbar Ar (instead of air) directly after deposition at 600°C (Figure 4.12) to provide information about the influence of oxygen during annealing. The AFM image shows that the Pt film was less segregated and formed a network instead of small islands. The height of the network reached up to 50 nm, except for a few particles that were larger than 100 nm. This is much flatter than the other sample. The oxygen environment seemed to contribute to the segregation process. Although it should be noted that the sample in Ar did not have the same annealing history.

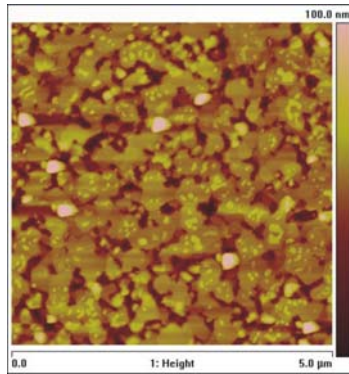


**Figure 4.12: AFM height image of YSZsc-Pt3 after annealing for 4 hours at 900°C in 0.25 mbar Ar**

#### 4.2.4 Results: Pt-paste

The Pt-paste was too rough to analyze with AFM, so SEM pictures were taken instead. At room temperature the pictures of the Pt-paste showed large rectangular shapes that were most likely some solvent residuals that disappeared during annealing. The platinum particles were very small but aggregated during annealing. After annealing at 900°C they formed one network of melted spherical particles.

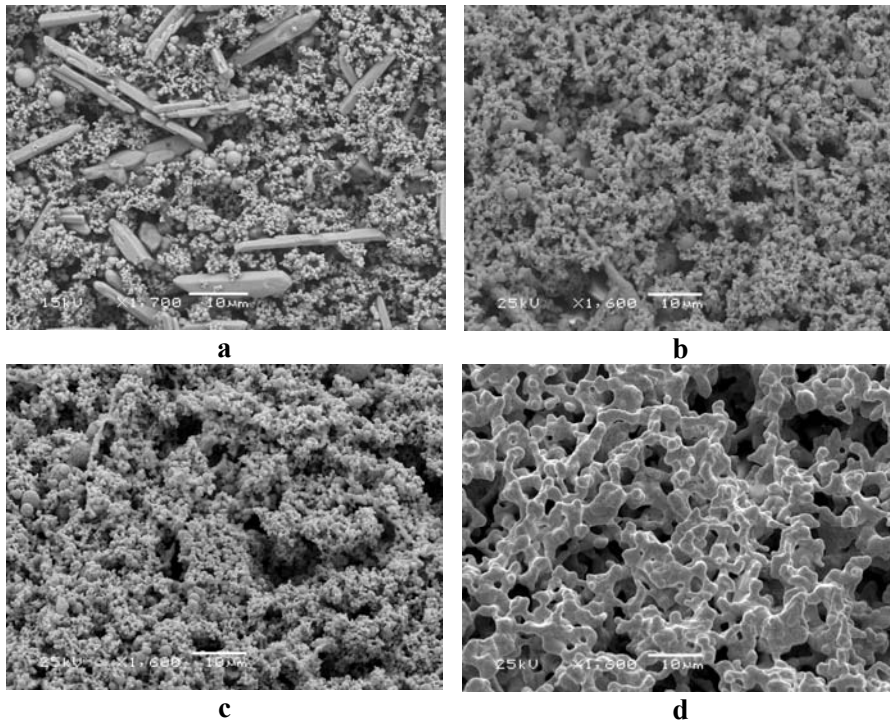


**Figure 4.13:** SEM picture on YSZsc-Pt-paste; a) as deposited, b) after annealing at 600°C, c) after annealing at 700°C; d) after annealing at 900°C

The porosity was so high after 900°C that in the optical microscope photos the substrate could be seen through the Pt-paste film at numerous places. It was very difficult to use wire bonding on this rough surface.

#### 4.2.5 Discussion and conclusions

Different electrode materials were studied to see their behaviour at high temperatures in oxygen environments. From the four electrodes SRO looks the most suitable. Despite the segregation, the SRO still seemed to remain a film. Au and Pt were segregated into islands, which can make the connection with the wire and the electrolyte weak and cause an increase in resistance as the contact area is decreasing. A solution to this segregation problem can be to increase the thickness of the films, but this increases the deposition time severely. The Pt-paste electrode was too porous and rough to be able to sustain a good bond.

### 4.3 Impedance measurements on a SRO electrode

The most suitable electrode material, SRO, was chosen for impedance measurement testing. To measure the behaviour of a SRO electrode during impedance measurements a sample was prepared with a 150 nm SRO film on YSZ (YSZsc-150SRO) and annealed for 6 ½ hours at 920°C. Four electrodes were etched in the SRO film. Two Au wires were bonded to the same electrode (Figure 4.14) to measure the electrode behaviour at several temperatures.

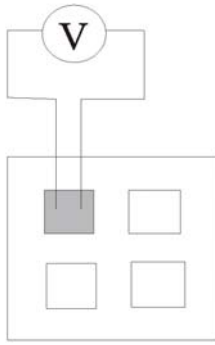


**Figure 4.14:** Schematic overview sample YSZsc-150SRO.

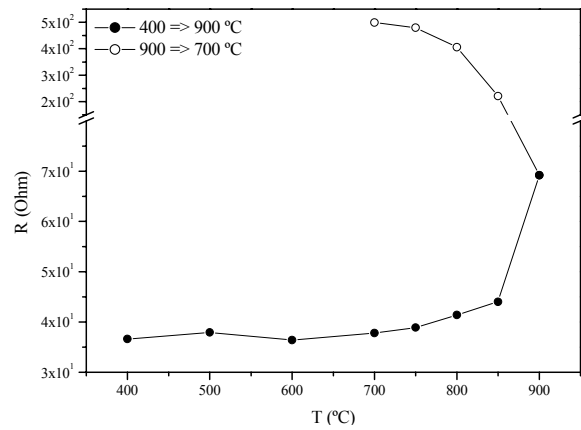


**Figure 4.15:** Resistance of YSZsc-150SRO at different temperatures measured with two Au wires bonded to one electrode.

Figure 4.15 shows that the resistance increased very little up to 850°C (36.6-44.0 Ohm), though from 800°C on the measurement became unstable (increasing resistance in time). At 900°C the resistance was significantly higher and the resistance kept increasing during cooling down, indicating a permanent change.

A possible reason for the increasing resistance is the reaction of the Au wire with the SRO film. The reaction with Ru is highly unlikely but with Sr it can react into intermetallic phases like AuSr, Au<sub>2</sub>Sr and Au<sub>5</sub>Sr (depending on the mole fractions)<sup>15</sup>.

Another reason can be that the segregation of the SRO film decreased the electrode contact area with the electrolyte as well as with the Au wire bond, leading to an increase in resistance.

This experiment shows that SRO electrodes can be used up to high temperatures (in this case ~800°C) before the resistance increases significantly.

## 5 YSZ: structure and composition

For the growth of YSZ films by PLD two 8 mol% YSZ targets were used. The first target was a 8 mol% YSZ single crystal target. The second target was made from 8 mol% YSZ powder, purchased at TOSOH. Results on XRD measurements on both targets and on films from both targets were compared and showed no difference. Also, XPS measurements were performed on a deposited YSZ film.

In this research reference samples were used with single crystalline 8 mol% YSZ substrates of  $5 \times 5 \times 0.5 \text{ mm}^3$  ordered from MTI Corp.. The exact synthesis procedure of these substrates was unknown, but the YSZ substrate had not undergone any additional heat treatment after synthesis. The substrate was oriented in the [001] direction (Figure 5.1 and Figure 5.2).

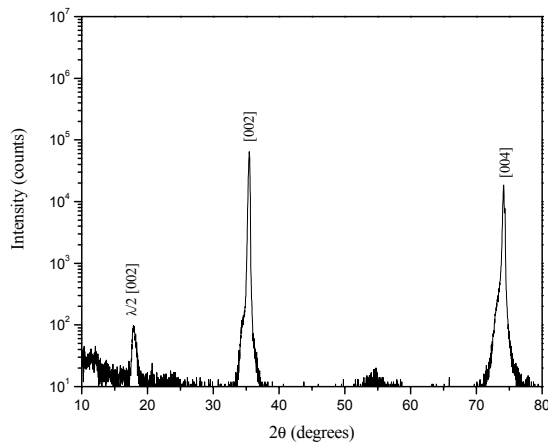


Figure 5.1: XRD of a single crystal YSZ substrate

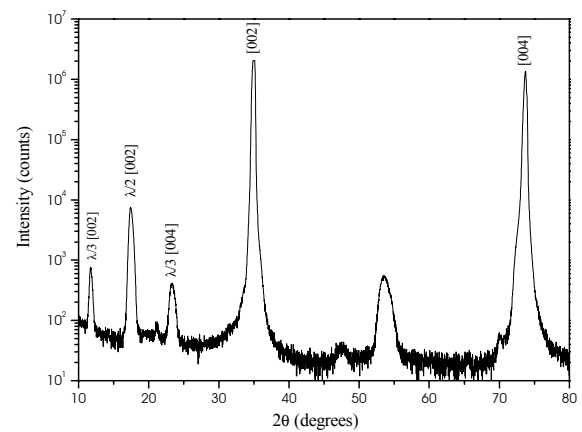


Figure 5.2: XRD of a single crystal YSZ substrate after 10 hours at 1400°C in air

After annealing, which was done to ensure stability during measurements, the XRD graph showed no structural changes in the YSZ.

### 5.1 Deposition parameters

The influence of the temperature and oxygen pressure, two important parameters during deposition, was studied. These parameters might be used to influence the crystallinity of the YSZ and hence the oxygen conductivity. The crystallinity was examined by XRD.

#### 5.1.1 Experimental

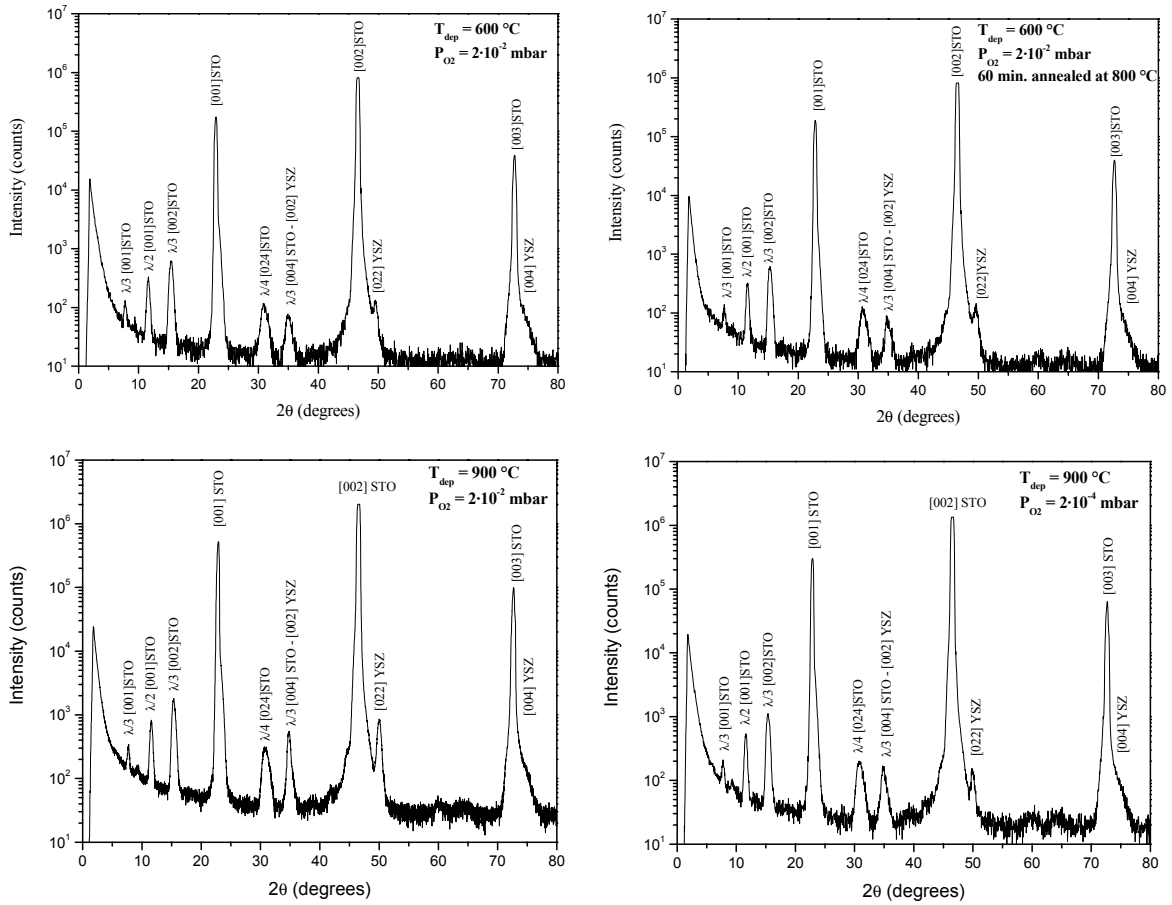
The YSZ depositions were done at 600°C and 900°C on a STO substrate. One sample deposited at 600°C was annealed for 60 minutes at 800°C. The depositions at 900°C were done in an oxygen pressure of  $2 \cdot 10^{-2}$  and  $2 \cdot 10^{-4}$  mbar (Table 5.1).

Table 5.1: Deposition parameters of YSZ on STO; fluency  $2.1 \text{ J/cm}^2$ , spot size  $3.36 \text{ mm}^2$ ,  $d_{\text{target,substrate}} = 59 \text{ mm}$ , frequency 7 Hz, 8 mol% YSZ target

Deposition temperature [°C]	Oxygen pressure [mbar]	Annealing
600	$2 \cdot 10^{-2}$	-
600	$2 \cdot 10^{-2}$	60 min. at 800°C
900	$2 \cdot 10^{-2}$	-
900	$2 \cdot 10^{-4}$	-

### 5.1.2 Results

The results are displayed in Figure 5.3.



**Figure 5.3: XRD graphs YSZ on STO; the small differences in peak intensity are attributed to the scanning parameters**

The [001] peaks of STO are clearly visible in the XRD graph exhibiting the highest intensities. The [022] YSZ peak is also clearly visible at  $2\theta = 50$  degrees. The [002] and [004] directions of YSZ coincide with STO peaks at  $2\theta = 34.9$  and  $73.7$  degrees. The diffraction patterns made with TEM (see chapter 5.1.3) confirmed the presence of the [001] directions in the sample deposited at  $900^\circ\text{C}$  in  $2 \cdot 10^{-2}$  mbar oxygen. From the other samples it was not proven that the [001] directions of YSZ were present. The possibility of a [111] YSZ peak at  $2\theta = 30.1$  degrees was excluded, instead this peak was assigned to the STO substrate.

The XRD graphs showed no clear dependence of the crystallinity on the temperature or the oxygen pressure.

## 5.2 TEM

A TEM image of a SRO-YSZ-SRO on STO-stack was made to see the crystallinity and growth behaviour of the films (Figure 5.4). The YSZ was deposited at 900°C in  $2 \cdot 10^{-2}$  mbar oxygen. The diffraction patterns confirmed the 45° rotation of YSZ on SRO.

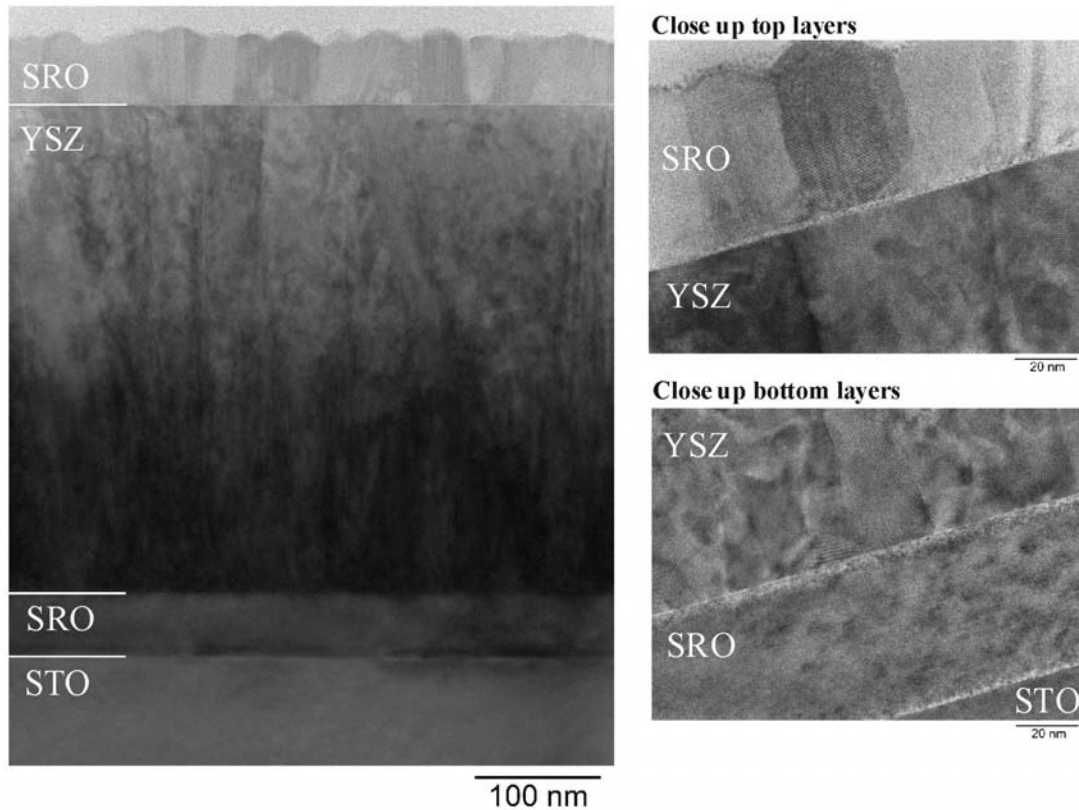


**Figure 5.4: TEM images of SRO/YSZ/SRO films on STO deposited by PLD**

The YSZ structure consisted of columnar grains grown in the deposition direction. Note that there is a contrast difference between the upper and lower part of the YSZ layer, but no evidence was found with XRD or XPS that the YSZ film altered during deposition.

The YSZ was deposited in the [001] direction, but the diffraction pattern could not confirm the presence of [011] directions as was found with the XRD scans in chapter 5.1.2.

The top SRO film consisted of grains in the same growth direction, indicating columnar growth. During deposition a number of nucleation points were formed instead of an initial smooth film. These nucleation points expanded in all directions until their boundaries met; then growth continued upwards.

According to the TEM results the films in the stack were grown epitaxially on each other.

### 5.3 XPS

XPS was used to measure the composition of the deposited YSZ films. The whole thickness of the film (300 nm) was examined and no large deviations were found concerning the yttria concentration. The atomic concentration of Y3d was  $6.6 \pm 0.8$  at%, which is very close to the target made from 8 mol% YSZ. The other concentrations can be found in Table 5.2 and Figure 5.5.

**Table 5.2: XPS results**

Element	Atomic concentration [%]	Error [%] <sup>c</sup>
Y3d	6.6	$\pm 0.8$
O1s	61.2	$\pm 1.1$
Zr3d	32.3	$\pm 2.0$

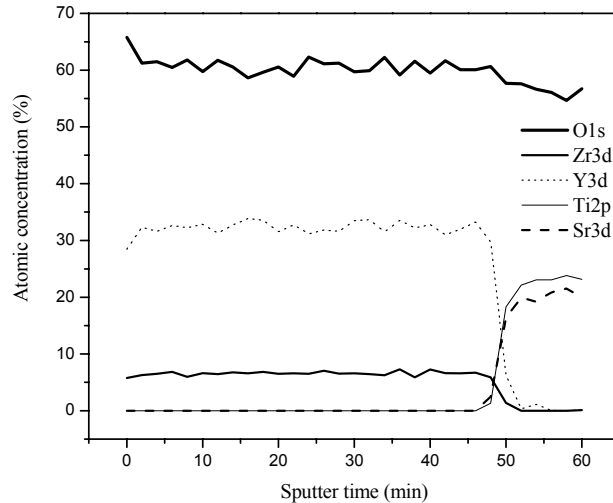


**Figure 5.5: XPS results of a 300 nm YSZ film on a STO substrate**

### 5.4 Discussion and conclusions

The YSZ structure was studied because of its influence on ionic conductivity measurements. The YSZ film consisted of columnar grains in the growth direction. The XRD showed the presence of [011] YSZ directions in all samples, but the presence of [001] directions could only be confirmed with TEM in one sample. No clear evidence was found that the crystallinity depended on the temperature or the oxygen pressure during deposition in the measured ranges. Therefore, these temperatures and oxygen pressures could not be used to alter the YSZ structure. The dopant concentration was, as expected, close to the concentration of the target.

<sup>c</sup> Maximum/minimum values found during measurements

## 6 YSZ: ionic conductivity

The objective of the ionic conductivity measurements was to determine the influence of the YSZ crystallinity on the oxygen conductivity. By changing the substrates on which YSZ is deposited, different crystal orientations could be obtained.

### 6.1 Impedance measurements with the Al-1%Si wire

Before finding out that the Al-1%Si wire was not suitable to measure in high temperatures, several measurements were already done. To find out if the resistance contribution from the Al-1%Si wire could be separated from the total resistance in these measurements, and thus obtain the YSZ resistance, a brief study was done. Unfortunately, no trend was observed in the additional resistance of the Al-1%Si wire and it was also uncertain if the wire resistance contribution was similar in each sample. This depends on the bonding strength and the progression of the decay.

#### 6.1.1 Stacks

Two stacks (Chapter 3.1) were deposited consisting of three films: SRO-YSZ-SRO on STO. In the first sample (stack178) the SRO films had a thickness of 39 nm and the YSZ film of 178 nm. The second sample (stack400) consisted of SRO films of 50 nm and an YSZ film of 400 nm. Figure 6.1 shows the impedance spectra of both stacks in the higher temperature regime. The spectra show clear bulk behaviour. The semi-circles in the impedance measurements were fitted with the equivalent circuit  $R_1Q_1$ .

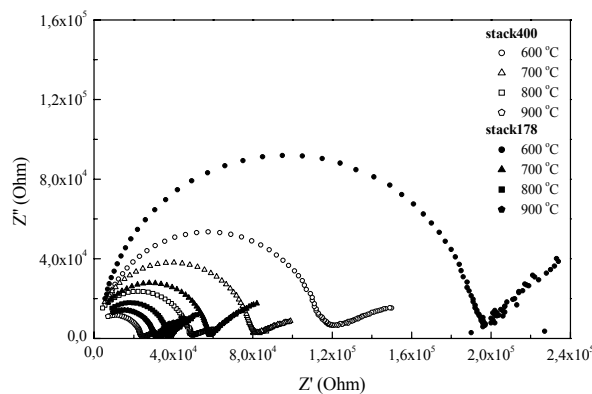


Figure 6.1: Impedance spectra stack178 and stack400 for the temperature range 600-900°C

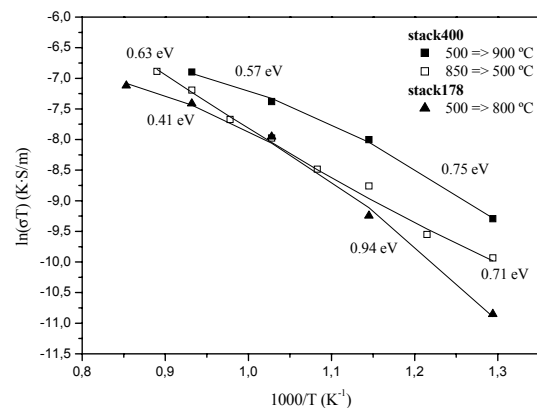
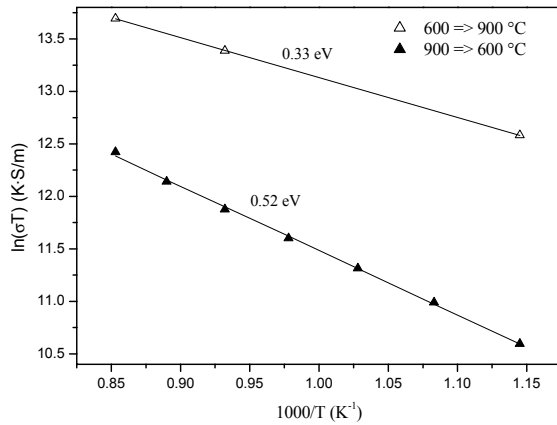


Figure 6.2: Arrhenius plots stack178 and stack400

Figure 6.2 gives the Arrhenius plots of both stacks. The activation energies of both stacks in the high temperature range (700-900°C) were 0.41 eV (stack178) and 0.57 eV (stack400). The ionic conductivities at 750°C were  $4.59 \cdot 10^{-9}$  and  $8.10 \cdot 10^{-9}$  S/cm, respectively, which was very low. The literature value lies around  $2 \cdot 10^{-3}$  S/cm for 10 mol% YSZ<sup>16</sup>. However it should be noted that the measurements were done while the sample had not been at the highest measuring temperature (900°C) yet. They were done while heating up to 900°C and therefore not stable. The values were also based on resistances, which contained a contribution of the Al-1%Si wire.

#### 6.1.2 Side electrode configuration

One measurement was done in the side electrode configuration (YSZ-Pt\_side), where the electrodes were placed next to the YSZ film (in plane). The electrodes were platinum instead of SRO because the deposition took place through a photo resist mask that should be kept below 100°C.



**Figure 6.3: Arrhenius plot YSZ-Pt\_side**

The activation energy of YSZ-Pt\_side was 0.33 eV in the high temperature range while heating up and 0.52 eV while cooling down. The ionic conductivity at 750°C was 6.6 S/cm, an unusual high value unlike the very low value found for the stack configuration. This confirms the unreliability of the Al-1%Si wire.

### 6.1.3 YSZ single crystals; instability in time

Two YSZ single crystal substrates were measured in time, one with Pt electrodes (YSZsc-Pt1) and one with 100 nm SRO electrodes (YSZsc-SRO1). None of the samples was annealed.

The measurements that were done during heating up were very unstable in time. Figure 6.4 and Figure 6.5 show the time dependence of the impedance spectra of YSZsc-Pt at 900°C.

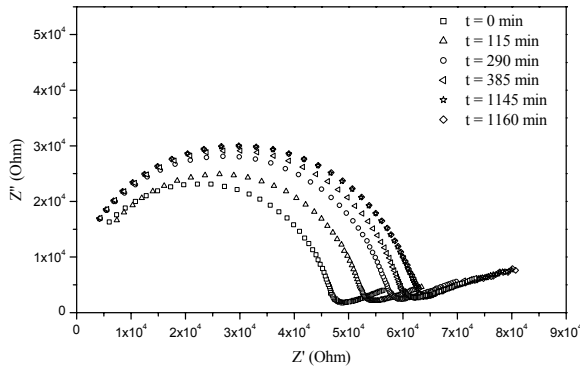


**Figure 6.4: Impedance spectra from YSZsc-Pt1 at 900°C; t is the start time of the measurement**

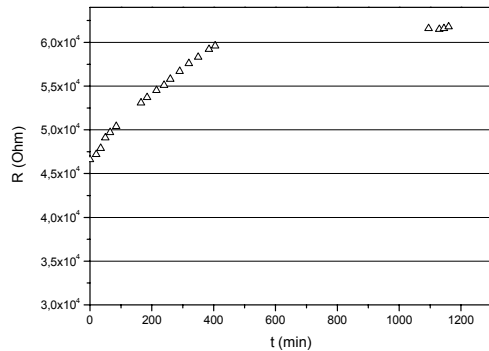


**Figure 6.5: Resistance in time**

The resistance of the sample was increasing with time towards a stable resistance. This behaviour was seen at every temperature. Instability due to temperature fluctuations in the sample was excluded. When the sample reached the maximum temperature of 900°C and its resistance was stable, the samples were cooled down and measured again. Now, no time dependency was observed. The fact that the sample (and especially the electrodes) had not been to these high temperatures yet probably played a large role in the unstable measurements.

The Arrhenius plots of YSZsc-SRO (Figure 6.6) confirmed that there was a large difference between measuring while heating up and cooling down. The points while cooling down were more accurate, resulting in a better fit ( $R^2=0.938$  for YSZsc-SRO1 from 700-850°C and  $R^2=0.9999$  from 850-700°C, fitted with a straight line). The ionic conductivities were very low ( $\sim 10^{-4}$ - $10^{-6}$  S/cm) indicating the measurements were influenced by electrode and/or wire behaviour.

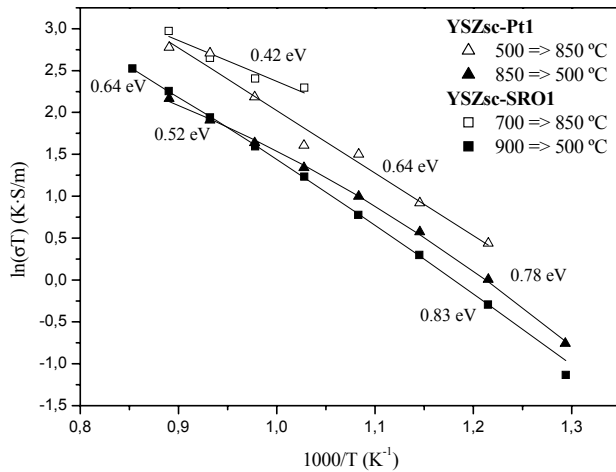


**Figure 6.6:** Arrhenius plots of YSZsc-SRO1 and YSZscPt1 during heating up and cooling down

In conclusion, it was clear that to measure accurate resistance values the whole sample should have been at the maximum temperature.

#### 6.1.4 Nitrogen/oxygen influence

On two YSZ single crystal substrates Pt-paste electrodes were applied in top electrode configuration. The first one was measured without annealing (YSZsc-Ptp1). In the second sample the YSZ substrate was annealed for 10 hours at 1400°C and an additional 2 hours at 800°C after applying Pt-paste electrodes (YSZsc-Ptp2).

These samples were used to discover the influence of N<sub>2</sub> on the measurements. The measurements were started in oxygen gas after which the gas was switched to nitrogen gas with the same flow rate. The measurements at 900°C were done while heating up the sample, the measurements at 750°C while cooling down.

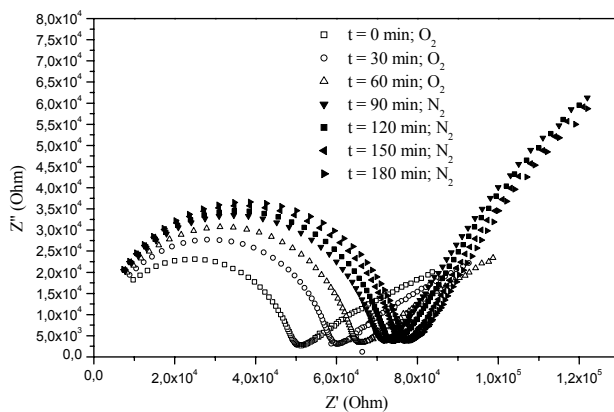


**Figure 6.7:** Impedance spectra YSZsc-Ptp1 in oxygen and nitrogen gas at 750°C; t is the start time of the measurement

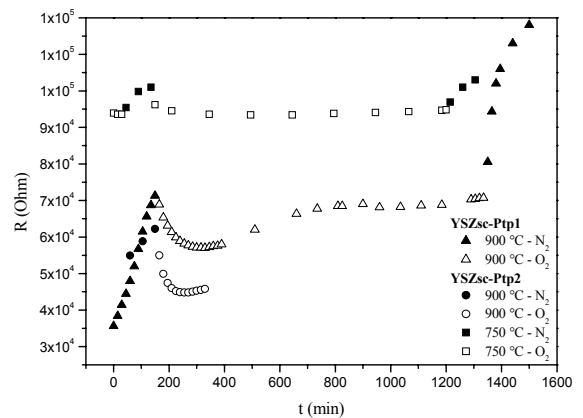


**Figure 6.8:** Resistance in time

The time dependency of the resistance was again clearly visible in Figure 6.7. The electrode behaviour changed when switching to nitrogen gas. Every time a switch was made an increase in bulk resistance was observed (Figure 6.8) regardless of the sample was heated up or cooled down. The YSZ resistance is P<sub>O<sub>2</sub></sub> independent thus the resistance difference must be caused by an additional resistance, indistinguishable from the bulk resistance in the impedance graphs. The change in resistance was considerable less when the sample was annealed. This confirmed that the cause was to be found in electrode behaviour. The annealing temperature of 800°C was below the maximum measuring temperature and the usual annealing temperature of Pt-paste (~900-950°C), therefore the Pt electrode could still have been unstable

at 900°C. New experiments should be done after annealing the Pt electrode at a temperature above 900°C, this should eliminate the nitrogen influence.

### 6.1.5 Discussion and conclusion

The Al-1%Si wire measurements were not suitable to provide clear information about the ionic conductivity due to the unknown influence of the electrode and wire resistance. For accurate measurements the whole sample should have been at the maximum temperature.

## 6.2 Impedance measurements with the Au wire

For the impedance measurements with the Au wires, all samples were first annealed at a temperature above 900°C. By using the Au wire, the wire and bond resistances were negligible in the measurements (Chapter 4.1) so only the resistance of the YSZ was being measured.

### 6.2.1 Reference samples

To verify if the system for measuring thin films was working correctly reference samples were measured by clamping them between two Au electrodes in larger oven. The first reference sample was made from a YSZ single crystalline substrate with on both sides Pt-paste electrodes, annealed at 700°C (YSZsc). The activation energy was 1.15 eV, measured in the temperature range of 400-800°C. This value is close to the value of ~1.1 eV found by Kosacki et al.<sup>3</sup> on a 10 mol% YSZ single crystal in the temperature range of 400-800°C. They also reported a decrease in activation energy above 650°C to ~0.9 eV even as Filal et al.<sup>17</sup> whom reported a change around 560°C. With the YSZsc sample similar behaviour was observed. The activation energy decreased to 1.06 eV, measured in the temperature range of 750-850°C. The oxygen conductivity of YSZsc was  $3.67 \cdot 10^{-2}$  S/cm, which is very close to the literature value of  $5.0 \cdot 10^{-2}$  S/cm<sup>16</sup> for 10 mol% YSZ.

The deviation in the activation energy depends on the structure of YSZ (grain size, morphology), thickness of the film and on the temperature range that is used to calculate the activation energy.

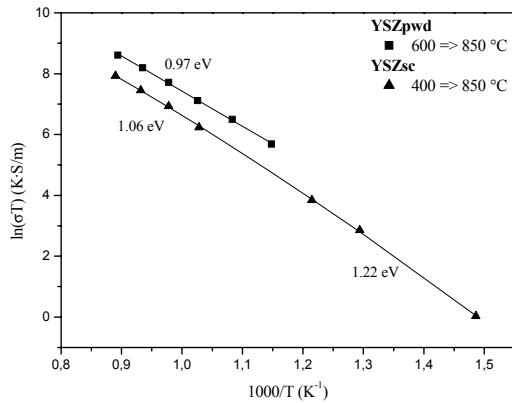


Figure 6.9: Arrhenius plots YSZsc and YSZpwd

Another reference sample was made from 8 mol% YSZ powder bought at TOSOH (YSZpwd). The sample had a density of  $5.94 \text{ g/cm}^3 \pm 0.01$  (~100% density) and was annealed for 5 hours at 1400°C. The crystallinity was not studied further. The sample was measured the same way as YSZsc. The activation energy was lower with 0.92 eV in the high temperature range, though the conductivity of  $7.25 \cdot 10^{-2}$  S/cm at 900°C was a little higher which can be caused by contaminations.

### 6.2.2 Single crystalline YSZ measurements

Four samples with an YSZ-substrate were prepared. On the first two a 200 nm SRO film was deposited and annealed for two hours at 920°C (YSZsc-SRO2 and YSZsc-SRO3). On the third sample a Pt film was deposited without annealing and the fourth sample with annealing for 4 hours at 900°C (YSZsc-Pt2 and YSZsc-Pt3, respectively). The impedance measurements can be found in Figure 6.10 and Figure 6.11.

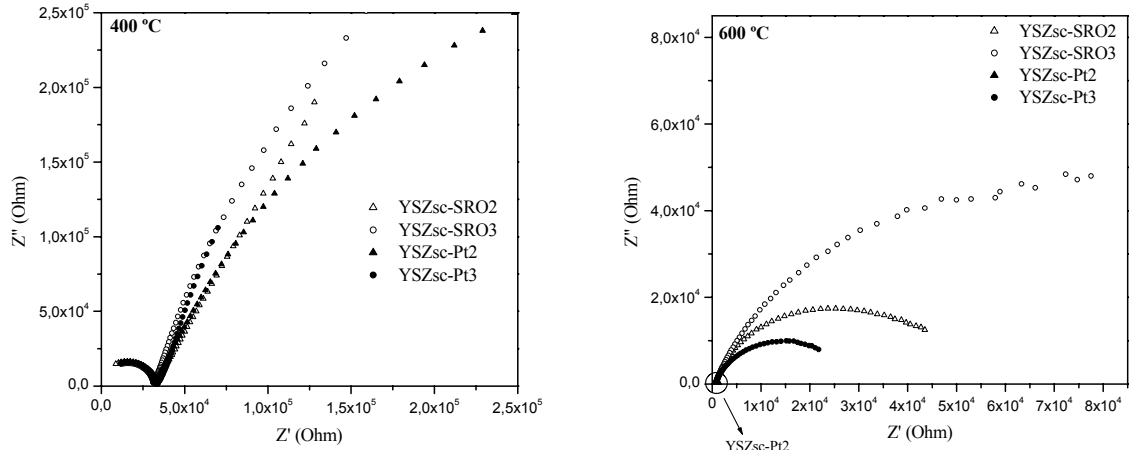


Figure 6.10: Impedance spectroscopy measurement results on the four samples at 400 and 600°C

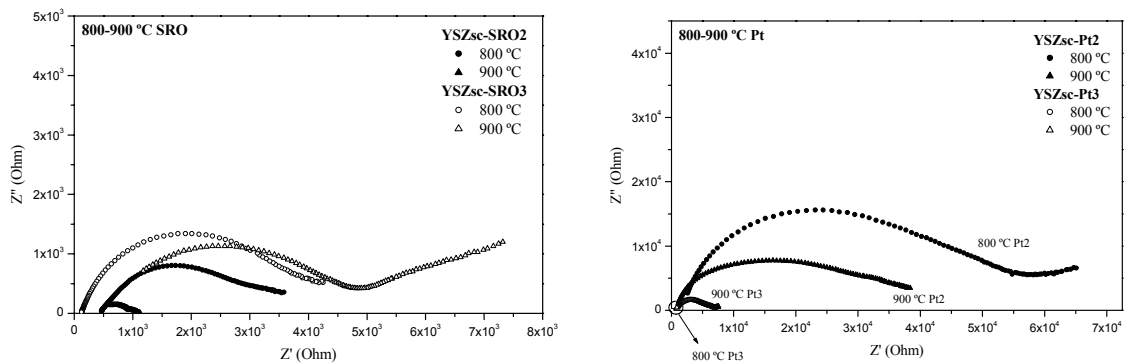


Figure 6.11: Impedance spectroscopy measurement results on the four samples at 800 and 900°C

At 400°C the impedance spectra were quite similar, even as the resistance. At 600°C the electrode behaviour started to change, though the bulk resistances were still similar. Around 750-800°C the electrodes started to segregate thereby influencing the measurements. For example while measuring YSZsc-Pt2 at 750°C the impedance spectra changed significantly in time, not only the resistance but also the shape of the graphs (Figure 6.12).

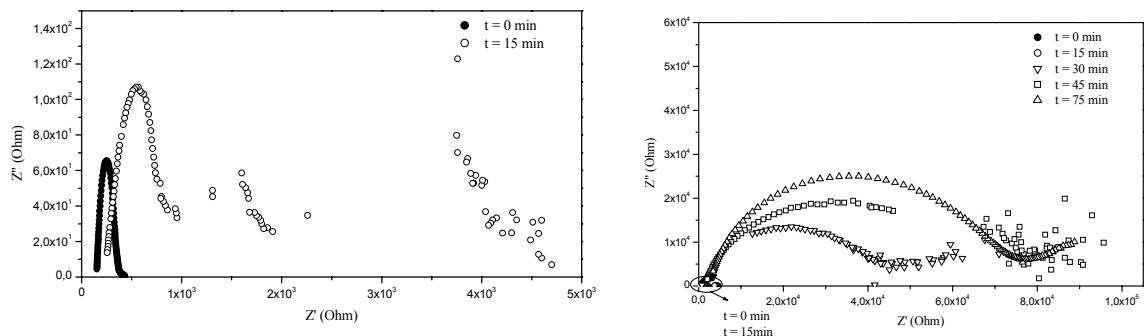
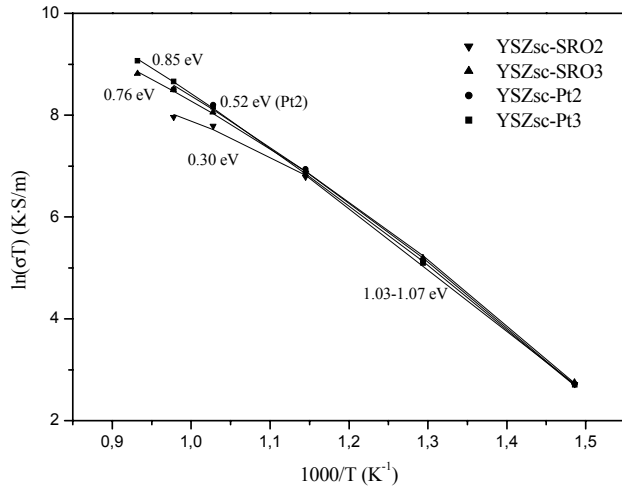


Figure 6.12: Impedance spectra YSZsc-Pt2 at 750°C; t is the start time of the measurement

After the change the resistance increased with increasing temperature, instead of decreasing, in three of the four samples. A decreasing electrode contact area with the electrolyte and wire bond could explain this unusual behaviour.



**Figure 6.13:** Arrhenius plots of YSZsc-SRO2, YSZsc-SRO3, YSZsc-Pt2 and YSZsc-Pt3;  $E_{act}$  = straight line fit 700-750°C

The activation energies of all four samples in the low temperature range (400-600°C) were between 1.03 and 1.07 eV (Figure 6.13). The values were expected to be the same in all samples because the electrolyte was similar. The electrodes should not influence the activation energy. Though at higher temperatures the activation energies differed largely from 0.60 to 0.88 eV at 750°C. These deviations agree with the results in Chapter 4, where the electrodes started to segregate at higher temperatures. Besides, the large deviation of YSZsc-SRO2 (Figure 6.13) could also be caused by the bond. It was difficult to bond Au to the very smooth SRO layer and therefore there could be differences between the strength of the bonds, which resulted in the unstable measurements at higher temperatures.

The ionic conductivities at 600°C varied from  $1.05 \cdot 10^{-2}$  to  $1.13 \cdot 10^{-2}$  S/cm, which is a little higher than the literature value ( $2.8 \cdot 10^{-3}$  S/cm for 10 mol% YSZ<sup>16</sup>) though 8 mol% YSZ should be a better ionic conductor. With a polynomial fit the data was extrapolated to calculate the ionic conductivities at 900°C, which resulted in values from  $1.09 \cdot 10^{-1}$  to  $1.65 \cdot 10^{-1}$  S/cm and for YSZsc-SRO2 of  $4.3 \cdot 10^{-2}$  S/cm. The value of YSZsc-SRO2 agreed well with the literature value ( $5 \cdot 10^{-2}$  S/cm<sup>16</sup>), however that was measured with 10-YSZ and thus the 8-YSZ value should be higher like the values found in the other measurements. Table 6.1 gives an overview of all the results.

**Table 6.1:** Over view activation energies and ionic conductivities

	YSZsc-SRO2	YSZsc-SRO3	YSZsc-Pt2	YSZsc-Pt3	Literature values 10%YSZ <sup>f,16</sup>
$E_{act,500}$ [eV]	1.00	1.03	1.05	1.04	-
$E_{act,750}$ [eV]	0.47	0.73	0.80	0.88	-
$\sigma_{400}$ [S/cm]	$2.24 \cdot 10^{-4}$	$2.30 \cdot 10^{-4}$	$2.22 \cdot 10^{-4}$	$2.19 \cdot 10^{-4}$	-
$\sigma_{600}$ [S/cm]	$1.05 \cdot 10^{-2}$	$1.13 \cdot 10^{-2}$	$1.11 \cdot 10^{-2}$	$1.08 \cdot 10^{-2}$	$2.8 \cdot 10^{-3}$
$\sigma_{750}$ [S/cm]	$2.95 \cdot 10^{-2}$	$4.69 \cdot 10^{-2}$	$5.15 \cdot 10^{-2}$	$5.56 \cdot 10^{-2}$	-
$\sigma_{900}$ [S/cm] <sup>g</sup>	$4.39 \cdot 10^{-2}$	$1.09 \cdot 10^{-1}$	$1.36 \cdot 10^{-1}$	$1.65 \cdot 10^{-1}$	$5.0 \cdot 10^{-2}$

<sup>f</sup> 8-YSZ has a higher conductivity than 10-YSZ; The ionic conductivity of 8-YSZ at 1000°C lies around  $1 \cdot 10^{-1}$  S/cm

<sup>g</sup> Values were calculated by a second order polynomial fit through data obtained in the temperature range 400-800°C

In conclusion, it was probably the segregation of the electrodes at high temperatures that influenced the measurements by changing the contact surface with the bond and/or the electrolyte. Thus the electrodes are reliable until 700°C. However, by extrapolating the data obtained at low temperatures, the conductivity at high temperatures can be calculated.

### 6.2.3 Thin YSZ films on NdGaO<sub>3</sub> and SrTiO<sub>3</sub>

A 300 nm YSZ film was deposited on a [001] NdGaO<sub>3</sub> substrate followed by a 150 nm SRO film as electrode (300YSZ-NGO). A top electrode configuration was etched in the SRO film and the sample was annealed for 3 ½ hours at 925°C. Figure 6.15 shows that YSZ was grown epitaxially on NGO in the [001] direction.

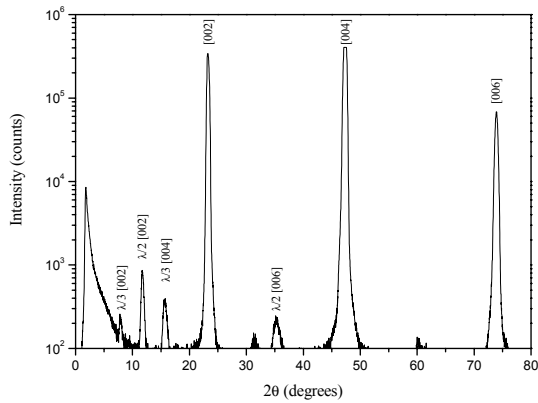


Figure 6.14: [001] NdGaO<sub>3</sub> substrate

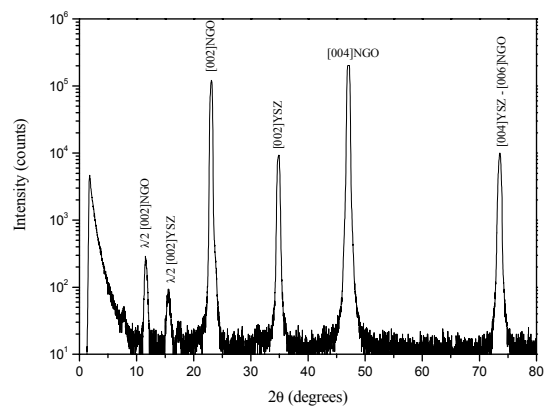


Figure 6.15: YSZ on a [001] NdGaO<sub>3</sub> substrate

A second sample was made similar to 300YSZ-NGO, but with a STO substrate instead of NGO (300YSZ-STO). The crystallinity of YSZ films on STO can be found in Chapter 5.

The impedance spectra of 300YSZ-NGO are in Figure 6.16 and Figure 6.17. Unfortunately the measurements while heating up were unstable in time. The data in the graphs are taken after 30 minutes stabilizing, though after 60 minutes the resistance was still increasing. The data taken during cooling down were not time dependent but differed largely from the measurements while heating up. Why this time-dependency is observed is not clear, the sample was annealed at 925°C, which should ensure stability up to 900°C. Only the Au wire has not been to this temperature, but other measurements with a Au wire were almost directly stable (300YSZ-STO). It might be that the bond was not well attached.

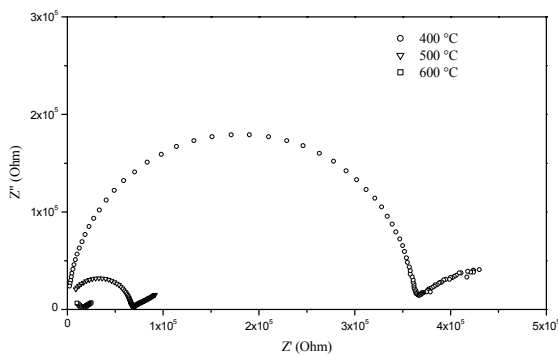


Figure 6.16: Impedance spectra 300YSZ-NGO; 400-600°C

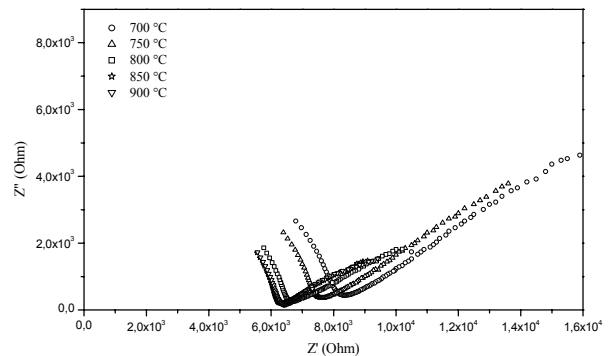


Figure 6.17: Impedance spectra 300YSZ-NGO; 700-900°C

Figure 6.18 shows the impedance data for 300YSZ-STO. From the temperature of 700°C the graphs clearly show grain boundary behaviour. Before this semi-circle a small onset of a semi-circle from bulk behaviour is visible. The bulk behaviour at high temperatures could (in these samples) only be measured at frequencies higher than 65 kHz, which was not possible with our equipment. So the high frequency intercept of the grain boundary response was used to determine the bulk impedance.

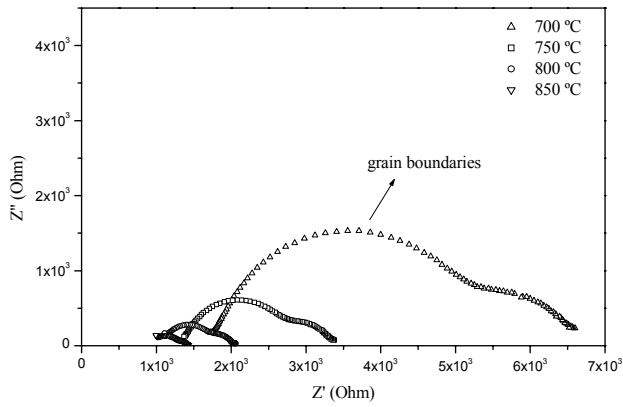


Figure 6.18: Impedance spectra 300YSZ-STO

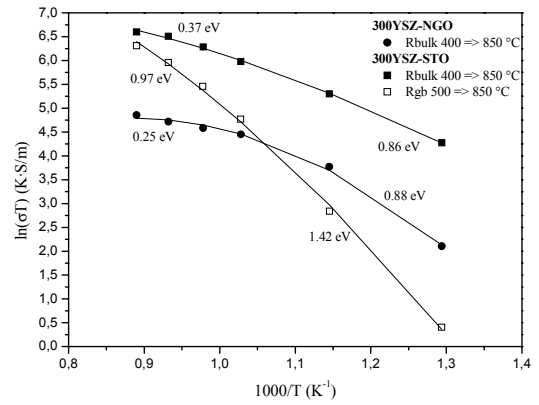


Figure 6.19: Arrhenius plots 300YSZ-NGO and 300YSZ-STO

TEM pictures showed (Figure 5.4) that the YSZ film grew in a columnar structure on SRO (and expected to grow the same on STO). In the top electrode configuration the ionic current was perpendicular to the growth direction of the columns, which might explain the observed grain boundary behaviour. The microstructure of the YSZ on NGO was not determined (due to lack of time) and might be different. Although no clear grain boundary behaviour was observed in these impedance graphs, there is the possibility that the grain boundary contribution was merged with the bulk impedance to one semi-circle. Kosacki et al.<sup>18</sup> report this phenomenon when the grain size decreases to the nanometer scale ( $< 100$  nm). A TEM picture should give more insight in the NGO structure.

The Arrhenius plots of both samples are displayed in Figure 6.19 and show that the activation energy changed at higher temperatures. The values found in the range of 700-850°C (0.37 eV for 300YSZ-STO and 0.25 eV for 300YSZ-NGO) were too low for ionic conduction. For example, Kosacki et al.<sup>3</sup> found a lowest value of 0.62 eV for 10-YSZ with a film thickness of 15 nm. An explanation could be that there was an additional series resistance contribution in this temperature range that could not be distinguished from the electrolyte resistance. Electronic contributions could also play a part. Electronic contributions can be caused by reactions at the interfaces or impurities. Interface reactions at these high temperatures are very likely to happen and can result in electronically conducting phases. Impurities were not found with XPS. Another option is still the influence of the electrode segregation.

Table 6.2 shows that the ionic conductivities of both samples were at least one order of magnitude lower than expected. This can be caused by the increased resistance due to an decreasing contact area of the electrodes. Comparing the ionic conductivities of both samples, the YSZ deposited on STO had a higher conductivity throughout the whole temperature range. An influence of the YSZ structure could have played part in this difference as the YSZ on NGO was deposited in the [001] directions and on STO in the [011] and [001] directions. For good comparison though, the measurements should be repeated.

Table 6.2: Overview results of 300YSZ-NGO and 300YSZ-STO

	300YSZ-NGO	300YSZ-STO bulk	300YSZ-STO grain boundaries
$E_{act, 400-600\text{ °C}}$ [eV]	0.88	0.86	1.42
$E_{act, 700-850\text{ °C}}$ [eV]	0.25	0.37	0.97
$\sigma_{400}$ [S/cm]	$6.84 \cdot 10^{-6}$	$2.00 \cdot 10^{-4}$	$3.73 \cdot 10^{-7}$
$\sigma_{600}$ [S/cm]	$4.33 \cdot 10^{-4}$	$2.33 \cdot 10^{-3}$	$2.23 \cdot 10^{-4}$
$\sigma_{750}$ [S/cm]	$9.93 \cdot 10^{-4}$	$5.10 \cdot 10^{-3}$	$2.11 \cdot 10^{-3}$
$\sigma_{900}$ [S/cm] <sup>h</sup>	$1.09 \cdot 10^{-3}$	$7.54 \cdot 10^{-3}$	$7.61 \cdot 10^{-3}$

<sup>h</sup> Data extrapolated to 900°C

The grain boundary conductivities had a higher activation energy (1.42 eV and 0.97 eV for 400-600°C and 700-850°C respectively) than the bulk (0.86 eV and 0.37 eV). The ionic conductivity was very low which could be expected as grain boundaries exhibit a blocking effect for ionic transport resulting in a specific grain boundary resistivity that could be several order of magnitude higher than the bulk conductivity<sup>19</sup>.

In conclusion, the measurements on thin YSZ films showed differences between deposition on STO and NGO. Grain boundary behaviour was only observed in 300YSZ-STO, however it could still be present in the 300YSZ-NGO sample. The activation energies of both samples were lower than expected. Electronic contributions can have contributed to that. The ionic conductivities were also very low; this was ascribed to the reduction of the contact area of the electrodes. The 300YSZ-STO sample had a higher conductivity than the 300YSZ-NGO sample, which might have to do with the difference in structure, though to draw hard conclusions the measurement should be repeated.

## 7 Discussion, conclusions and recommendations

### 7.1 Discussion and conclusions

The objective of this research was to determine the influence of the crystal structure on the oxygen conductivity of thin YSZ films produced by pulsed laser deposition. To be able to do so several obstacles had to be overcome. The Al-1%Si bonding wire, used for the first impedance measurements, turned out to be inapplicable at temperatures  $> 580^{\circ}\text{C}$ . Also parts of the sample-holder did not withstand the measurement conditions. For the Al-1%Si wire a replacement was found in a Au wire and in the sample-holder the oxidized parts were left out in a new design. The impedance measurements done with the Al-1%Si wire resulted in unrealistic values for the activation energies and ionic conductivities. The measurements showed that the sample should have been at the maximum measurement temperature before measurements.

The electrodes formed the next challenge. Four electrode materials were tested that initially seemed to fulfil the requirements (SRO, Pt, Au and Pt-paste). These materials were electrical conducting and porous enough to ensure oxygen transport through the electrode. They were tested on their behaviour at high temperatures. From the four tested electrode materials SRO was the most suitable at high temperatures. Despite some segregation, the SRO still seemed to form a film after annealing at  $900^{\circ}\text{C}$ . The Pt-paste was too porous and rough to be able to sustain a good bond. The Au and Pt films completely segregated into islands. Segregation of the film was unwanted because it reduces the contact area of the bonding wire and electrolyte with the electrode resulting in an increased resistance. An alternative might be to use thicker electrodes or dense Pt electrodes instead of porous Pt electrodes.

The impedance measurements with the Au wire were first tested on YSZ single crystal substrates with Pt or SRO electrodes on top. This sample configuration was chosen because it was relatively easy to make, though the exact geometry was not known which induced a possible deviation in the calculations. Therefore it is recommended to use sample configurations with known geometries, for example the stack configuration.

At low temperatures the activation energies of the YSZ single crystal substrates were quite similar and agreed with literature values. Though from a temperature around  $750\text{-}800^{\circ}\text{C}$  the measurements (as well with Pt as with SRO electrodes) became instable, which was attributed to the segregation of the electrodes. Thus SRO and Pt electrodes are only applicable up to a temperature of  $700^{\circ}\text{C}$ .

YSZ thin films were measured deposited on STO as well as on NGO. The activation energies of 0.86 and 0.88 eV in the temperature range of  $400\text{-}600^{\circ}\text{C}$  were lower than the values found in literature which were  $\sim 1$  eV. In the high temperature range, the activation energies became very low. Other conduction mechanisms can have played a part in this, like electronic conduction. The ionic conductivities at  $750^{\circ}\text{C}$  were  $5.10 \cdot 10^{-3}$  and  $9.93 \cdot 10^{-4}$  S/cm, respectively, at least one order of magnitude lower than expected. Here the influence of the electrode segregation is visible again. An influence of the YSZ structure could have played part in the ionic conductivity difference as the YSZ on NGO was deposited epitaxial in the [001] directions and on STO in the [011] and [001] directions. For good comparison though, the measurements should be repeated.

In conclusion, the use of thin films able to withstand high temperatures in an oxygen environment provided several challenges concerning the bonding wire and electrode materials. A good bonding wire was found in gold wiring, though the search for even better ones continues. SRO and Pt electrodes turned out to be only applicable up to  $700^{\circ}\text{C}$ , thus for higher temperatures other electrodes need to be found. However, the results obtained from low temperature measurements can be extrapolated to high temperatures to get an indication

of the values. For conductivity calculations it is important to have a known geometry in the sample configuration to avoid large deviations. At this moment no clear answer can be given on the question how the crystal structure of YSZ influences the ionic conductivity.

## 7.2 Recommendations

After all the obstacles while finding the right way to measure the YSZ ionic conductivity, little time was left to actually measure the ionic conductivity well. Therefore, the best recommendation is to continue where the measurements left off by extending the measurements on YSZ thin films deposited on STO and NGO, but also on other substrates (for example Si) and find out more about the influence of the crystallinity on the ionic conductivity.

Other recommendations are listed below.

- Optimise the sample configuration further to a configuration with a known geometry which can be deposited *in situ* or in less steps (reducing contamination);
- Search for electrode materials that do not segregate (or less) at high temperatures, for example dense Pt films, or increase the thickness of the electrodes;
- Reduce the measurement temperatures and extrapolate the data to the high temperature region;
- Use higher frequencies (> 65 kHz) during impedance measurements to see bulk behaviour at high temperatures.

## Dankwoord

In de negen maanden dat ik bezig ben geweest met mijn afstudeeropdracht heb ik met veel plezier deel uit gemaakt van de vakgroep Anorganische Materiaalkunde. Het was een erg gezellige groep en ik kon bij iedereen aankloppen om even een praatje te maken of om advies te vragen.

Natuurlijk wil ik mijn commissie bedanken voor hun inzet, begeleiding en advies. Als eerste wil ik Frank bedanken, mijn directe begeleider, om deel uit te mogen maken van zijn promotieonderzoek. Het was erg prettige samenwerking en ik heb er veel van opgestoken. Guus bedankt voor de besprekingen en discussies. Dave bedankt voor je enthousiasme en gastvrijheid. Henny bedankt voor je nuttige bijdragen vanuit de CT-kant. Bart Jan en Björn bedankt voor de interesse en de tijd die jullie in mijn scriptie hebben gestoken. Bernard bedankt voor je hulp bij het uitwerken van de impedantie metingen. Ook dank aan alle andere mensen bij AMK en MESA+ die hebben bijgedragen aan mijn afstudeerproject en aan de gezellige koffiepauzes.

Ik wil natuurlijk ook mijn afstudeercollega's bedanken die samen met mij probeerden het hoofd koel te houden in onze afstudeerkamer (letterlijk en figuurlijk). Ook hebben ze mij het een en ander over cryptogrammen bijgebracht, zodat ik nog altijd prijspuzzels kan gaan oplossen als ik niet direct werk vind...

En last but not least, mijn ouders die altijd voor me klaar stonden en Mark die zorgde dat ik af en toe wat rust nam en er altijd voor me was.

Allemaal heel erg bedankt!



Jetske Stortelder  
18 augustus 2005

## Literature

---

- <sup>1</sup> P.J. Gellings and H.J.M. Bouwmeester, *The CRC handbook of solid state electrochemistry*, CRC press, Inc, Florida, 1996
- <sup>2</sup> P. Mengucci, et al., *Effects of annealing on the microstructure of yttria-stabilised zirconia films deposited by laser ablation*, Thin Solid Films 478, 125-131 (2005)
- <sup>3</sup> I. Kosacki, et al., *Nanoscale effects on the ionic conductivity in highly textured YSZ thin films*, Solid State Ionics 176, Issues 13-14, 1319-1326 (2005)
- <sup>4</sup> P.S. Manning, et al., *The kinetics of oxygen transport in 9.5 mol % single crystal yttria stabilised zirconia*, Solid State Ionics 100, 1-10 (1997)
- <sup>5</sup> I. Kosacki, V. Petrovsky and H.U. Anderson, *Modelling and characterization of electrical transport in oxygen conducting solid electrolytes*, Journal of Electroceramics 4:1, 243-249 (2000)
- <sup>6</sup> C. Haering, A. Roosen and H. Schichl, *Degradation of the electrical conductivity in stabilized zirconia systems Part I: yttria-stabilized zirconia*, Solid State Ionics 176, 253-259 (2005)
- <sup>7</sup> Gamry Instruments, *Electrochemical impedance spectroscopy primer*, [http://www.gamry.com/App\\_Notes/EIS\\_Primer/EIS\\_Primer.pdf](http://www.gamry.com/App_Notes/EIS_Primer/EIS_Primer.pdf), June 2005
- <sup>8</sup> A.J.H.M. Rijnders, *The initial growth of complex oxides: study and manipulation*, Proefschrift Universiteit Twente, Enschede, 2001
- <sup>9</sup> I.N. Shklyarevskii and P.L. Pakhmov, *Separation of the contribution of free and bound electrons into real and imaginary parts of the dielectric constant of gold*, Optika i Spektroskopiya 34(1), 163-166 (1973)
- <sup>10</sup> F. Cardelli, *Materials Handbook*, Springer-Verlag London Limited, 2000
- <sup>11</sup> Marketch International Inc., <http://www.mkt-intl.com/superconductor/single.htm>, August 2005
- <sup>12</sup> J.H. Westbrook (editor), *Moffatt's handbook of binary phase diagrams*, Genium publishing corporation, New York, August 1997
- <sup>13</sup> H.C. Choe, et al., *Early stage heteroepitaxial growth of SrRuO<sub>3</sub> films on SrTiO<sub>3</sub> (001) depending on the growth temperature during pulsed laser deposition*, Thin Solid Films 474, 44-49 (2005)
- <sup>14</sup> X. Zhu, et al., *Microstructure of (110)-oriented epitaxial SrRuO<sub>3</sub> thin films grown on off-cut single crystal YSZ (100) substrates*, Materials Science and Engineering B 118, Issues 1-3, 60-65 (2005)
- <sup>15</sup> R.A. Alqasmi, *Thermodynamics of solid Au-Sr alloys*, Journal of Alloys and Compounds 292, 148-151 (1999)
- <sup>16</sup> B.C.H. Steele, *Ceramic ion conducting membranes*, Current Opinion in Solid State & Materials Science 1, 684-691 (1996)

<sup>17</sup> M. Filal, et al., *Ionic conductivity of yttrium-doped zirconia and the “composite effect”*, *Solid State Ionics* 80, 27-35 (1995)

<sup>18</sup> H.L. Tuller, *Ionic conduction in nanocrystalline materials*, *Solid State Ionics* 131, 143-147 (2000)

<sup>19</sup> X. Guo and J. Maier, *Grain boundary blocking effect in zirconia: A Schottky Barrier analysis*, *Journal of The Electrochemical Society* 148 (3), E121-E126 (2001)

## Appendix I: Geometry calculations for the top electrode configuration

For ionic conductivity calculations the geometry of the sample had to be determined because the ionic conductivity is given by the relationship:

$$\sigma = \frac{d}{RA} \quad (0.1)$$

With  $d$  the path length of the current and  $A$  the electrode surface. Each sample deposited in the top electrode configuration was made using the same mask. Therefore, only the path length varied.

The electrode surface was defined as the surface where the potential  $> 0$ . In this case the influence of the potential was only of importance when the current density is sufficiently high ( $\gg 0$ ).

Figure A.1 gives an schematic impression of the electrode surface and the path length as used in the calculations.

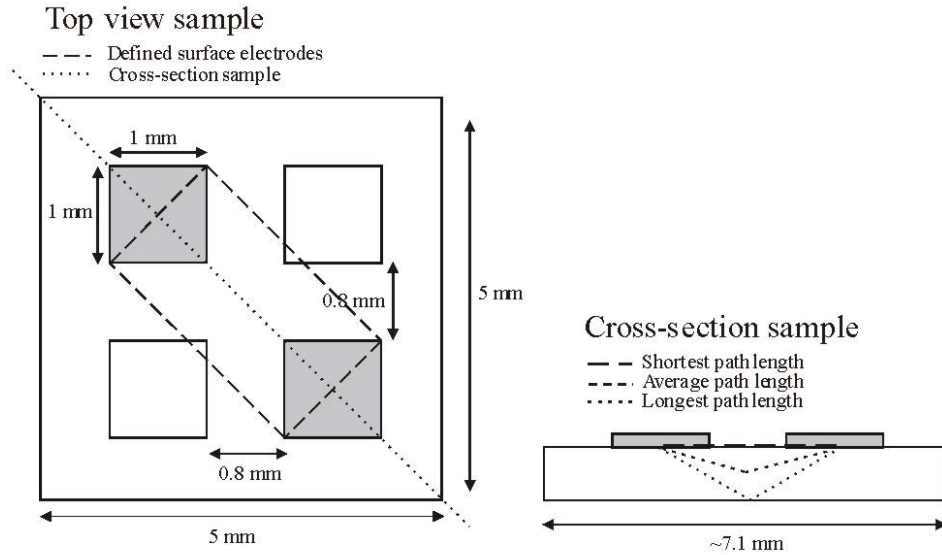


**Figure A.1: Schematic view of the electrode surface and the current path length**

The electrode surface was estimated as a rectangle with width  $a$  and length  $b$ :

$$a = \sqrt{2} \quad (0.2)$$

$$b = 2 \cdot 0.5\sqrt{2} + \left( \sqrt{0.8^2 + 0.8^2} \right) \approx 2.55 \text{ mm} \quad (0.3)$$

The electrode surface was  $3.6 \text{ mm}^2$  for the top electrode configuration.

The shortest path length equalled  $b$  (equation (0.3)) and the longest path length equalled:

$$\text{longest\_path\_length} = 2\sqrt{(0.5b)^2 + (\text{layer\_thickness})^2} \quad (0.4)$$

From both path lengths an average was calculated which resulted in an average path length of  $2.64 \text{ mm} = 2.64 \cdot 10^{-3} \text{ m}$  in case of an YSZ single crystal substrate with a thickness of  $0.5 \text{ mm}$ .

This approach was an estimation of the geometry, because an exact value for the path length and electrode surface requires experiments to determine how the current and potential densities are spread. Available methods for these calculations require that the thickness of the electrodes is much larger than the thickness of the sample, which is not the case here, and are most often two-dimensional, neglecting a vertical current path possibility.

The geometry of the samples only affected the ionic conductivity, not the activation energy. A calculation was done to estimate the impact of the geometry values on the ionic conductivity. The path length and electrode surface were varied while calculating the ionic conductivity. The influence of both parameters was equal, though the estimated error was different. The limits for the path length were the longest and shortest path length ( $\pm 3.5\%$ ) and for the electrode surface an error of  $\pm 40\%$  was taken.

The error in the conductivity caused by the path length was at most 0.6% (calculated with ionic conductivities at 600°C) and for the electrode surface at most 7.4%. Combining the limits of both parameters resulted in a maximum error of 7.8% at 600°C. The data in the Arrhenius plot was fit with a second order polynomial, which resulted in a decrease of the error at higher temperatures (e.g. the maximum error at 400°C is 16.6% and at 750°C 6.0%).